Geochimica et Cosmochimica Acta 368 (2024) 34–49

Contents lists available at ScienceDirect

Geochimica et Cosmochimica Acta

journal homepage: www.elsevier.com/locate/gca

Silicon isotopes in an Archaean migmatite confirm seawater silicification of TTG sources

Madeleine E. Murphy *, Jane E. Macdonald, Sebastian Fischer, Nicholas J. Gardiner, Richard W. White, Paul S. Savage

School of Earth and Environmental Sciences, University of St Andrews, Bute Building, Queen's Terrace, St Andrews KY16 9TS, Scotland, United Kingdom

ARTICLE INFO

Associate editor: Janne Blichert-Toft

Keywords:
Archaean
TTG
Si isotopes
Migmatites
Silicification

ABSTRACT

Unraveling ancient melting processes is key to understanding how the earliest, tonalite-trondhjemite-granodiorite (TTG)-dominated continental crust formed from partial melting of amphibolite. Application of silicon isotope analysis to ancient crust reveals that Archaean TTGs exhibit consistently high Si isotope values (δ^{30}Si) compared to modern granitoids, attributed to seawater-derived silica introduced by either (a) partial melting of variably silicified basalts or (b) assimilation of authigenic silica-rich marine lithologies in the melt source. However, both mechanisms can introduce highly variable δ^{30}Si, conflicting with the strikingly consistent δ^{30}Si compositions of Archaean TTGs. This study investigates an alternative model, whereby the distinct mineralogy and chemistry of TTG melt sources impart a distinct silicon isotope composition to the melt, compared with "modern" granitoids. We measured δ^{30}Si in component parts (melanosome and leucosome) of an Archaean (2.7 Ga) mafic migmatite and coeval amphibolites and mafic granulites from the Kapuskasing uplift, Canada, to explore how Si isotopes fractionate during incipient TTG melt formation. Our data reveal leucosome (i.e., melt) exhibits consistently high δ^{30}Si values compared to a relatively isotopically lighter melanosome (i.e., residuum). We also derive inter-mineral silicon isotope fractionation factors for mineral separates that agree well with those of *ab initio* estimates for the same minerals and show that the magnitude of equilibrium fractionation between TTG source rock and melt replicates that in Phanerozoic granitoids. We conclude the effects of magmatic differentiation on δ^{30}Si have remained consistent throughout Earth history, meaning that Archaean TTGs must require a source isotopically heavier than unaltered basalt, as reflected by our amphibolites and mafic migmatite components. The consistently heavy δ^{30}Si of seawater through Earth history, and the high SiO_2 content of amphibolites relative to coeval leucosome-free granulites in our study area, imply seawater silicification is the source of the observed high δ^{30}Si. Thus, the consistently heavy Si isotope compositions measured in Archaean melt products define a unique aspect of ancient crust formation: that of the silicification of TTG source rock, implying the intrinsic involvement of a primeval hydrosphere.

1. Introduction

The mechanisms involved in the genesis of the earliest continental crust, predominantly composed of the Archaean tonalite-trondhjemite-granodiorite (TTG) suites, continue to spark debate regarding early Earth geodynamic processes. While there is consensus that TTGs formed from the partial melting of hydrated (meta)basaltic source rocks (e.g., Foley et al., 2002; Moyen & Martin, 2012; Rapp & Watson, 1995), there is limited consensus on the geodynamic conditions under which these amphibolites melted. To clarify both melting regime(s) and putative sources during TTG petrogenesis, many approaches have been taken–including the application of several different stable isotope systems. For example, Fe isotopes have been employed to elucidate ancient precursor material and investigate mantle involvement and depth of Archaean gneiss formation (Dauphas et al., 2004; Doucet et al., 2020; Liou et al., 2022), O isotopes have pointed to the presence of a terrestrial magma ocean and emphasised the extent of a hydrosphere in generating early crust (Bindeman & O'Neil, 2022; Rumble et al., 2013; Smithies et al., 2021), and recent Ti isotope studies have been used to debate the onset of >3.5 Ga plate tectonics and establish a new tool to investigate geodynamic settings of magmatism (Greber et al., 2017; Deng et al., 2019b; Aarons et al., 2020; Hoare et al., 2020).

* Corresponding author.
E-mail address: mm439@st-andrews.ac.uk (M.E. Murphy).

https://doi.org/10.1016/j.gca.2024.01.018
Received 2 June 2023; Accepted 17 January 2024
Available online 24 January 2024

Recently, the application of stable silicon isotopes have revealed that Archaean TTGs consistently exhibit heavy silicon (Si) isotope values compared to Phanerozoic (i.e., 'modern') granitoids (Fig. 1; André et al., 2019; Deng et al., 2019a), with this offset appearing remarkably consistent both spatially and temporally. This small but significant difference is attributed to the presence of seawater-derived silica in the TTG melt source, introduced by either (a) anatexis of variably silicified basalts (André et al., 2019, 2022) or (b) assimilation of authigenic silica-rich marine lithologies (Deng et al., 2019a). However, both mechanisms can involve processes and sources that generate highly variable Si isotope compositions (Fig. 1); unsilicified to silicified metabasalts exhibit a large range in δ^{30}Si values (André et al., 2019; Abraham et al., 2011), and Archaean cherts can have a wide range of signatures, including very negative values (see Fig. 1 and sources therein), depending on their origin as diagenetic, hydrothermal, or silicified (Marin-Carbonne et al., 2012). The large range in Si isotope values generated by the processes that form these inferred source rocks conflicts with the strikingly consistent, high δ^{30}Si values observed in Archaean TTGs.

This study firstly investigates an alternative mechanism, whereby silicon isotopes fingerprint a distinct process inherent to the chemistry/conditions of Archaean TTG melt formation compared to "modern" crustal melting (i.e., the formation of Phanerozoic granitoids). While there are estimated *ab initio* fractionation factors for silicon isotopes from first-principles experimental studies (Méheut et al., 2009; Huang et al., 2014; Méheut and Schauble, 2014; Qin et al., 2016; Li et al., 2020; Rabin et al., 2021), there is a paucity of reported Si isotope fractionation factors between igneous/metamorphic minerals and coeval melt in natural samples (Guitreau et al., 2022; Li et al., 2020; Savage et al., 2011).

To this end, we aim here to elucidate Si isotope fractionation during incipient TTG melting, which requires a sample set that preserves the components of melted Archaean material. An ideal case study to address this knowledge gap is the ~2.7 Ga Kapuskasing uplift, Ontario, as its mafic migmatites include preserved melting components, as well as amphibolitic material thought to represent the source rock that melted to produce TTGs in the area. Specifically, the uplift is thought to represent a tilted section of Archaean crust (e.g., Percival et al., 2012), allowing investigation of lower crustal granulites and mid-crustal amphibolites, the protoliths of which are coeval and interpreted to be cogenetic (Hartel & Pattison, 1996). This exposure allows us to deconstruct the melting process at the Kapuskasing uplift by measuring Si isotopes in whole-rock amphibolites, granulite facies gneisses, and the components of migmatites, as well as in mineral separates from these rocks, to explore the fractionation of silicon isotopes during Archaean crustal melting.

This study thus presents the first empirically determined inter-mineral Si isotope fractionation factors for quartz, plagioclase, clinopyroxene, hornblende, and garnet from natural Archaean samples as well as bulk Si isotope values for these rocks. From these results we show that the effects of magmatic differentiation on Si isotopes have remained consistent throughout Earth history. Further, reflecting the global trend in Archaean TTGs, our amphibolites and the components of our mafic migmatite have high δ^{30}Si compared to modern analogues. We also see an isotopic difference between the amphibolitic and migmatitic TTG source rocks and their coeval granulite facies (but leucosome-free) equivalents. This heavy Si isotope character of melted Archaean rocks, along with the high silica content of the amphibolites relative to their coeval granulite counterparts, is interpreted here to reflect the innate involvement of seawater in silicifying and hydrating the mafic source rocks to Archaean TTGs.

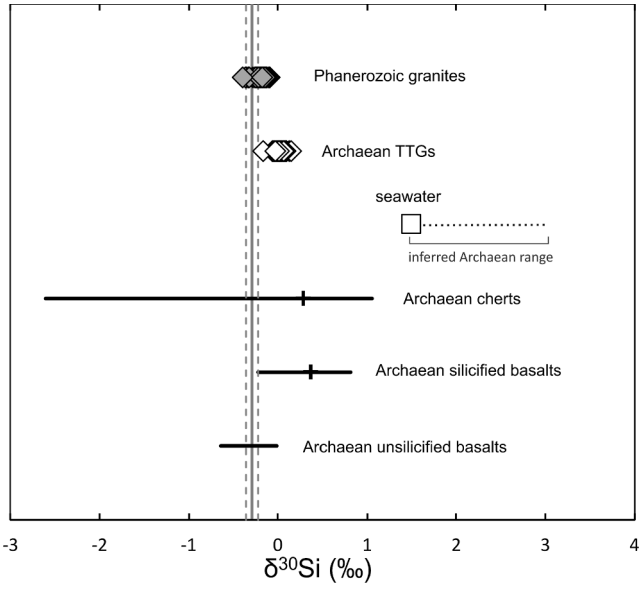

Fig. 1. Range in silicon isotope values for Archaean TTGs (André et al., 2019; Deng et al., 2019a) and the materials inferred to have imparted their high δ^{30}Si values, relative to Phanerozoic granites (Savage et al., 2012; Poitrasson and Zambardi, 2015). These include variably silicified and unsilicified Archaean basalts (André et al., 2019; Abraham et al., 2011) and Archaean cherts (Robert and Chaussidon, 2006; van den Boorn et al., 2007; 2010; Marin-Carbonne et al., 2012; Stefurak et al., 2015). Also depicted is the δ^{30}Si composition of modern seawater (white square, from Sutton et al., 2018) and the range of inferred values for Archaean seawater (dotted line; Sun et al., 2023; Stefurak et al., 2015). Black vertical tick marks show average value for each data range. The grey line and 2 s.d. dashed error bars represent the bulk silicate Earth (BSE) value of –0.29 ± 0.07 ‰ (after Savage et al., 2014).

2. Geologic background and samples

2.1. Geologic background

The samples in this study were collected from the Kapuskasing uplift, located in Ontario in the southern portion of Canada's Archaean Superior Province (Fig. 2). The Superior Province in Canada consists of east-west-running volcanic and sedimentary belts known as subprovinces, including the Abitibi and Wawa subdomains, which comprise supracrustal volcanics postulated to have formed in an oceanic arc, with peak magmatism occurring at 2730–2700 Ma (Percival et al., 2012; Percival and Card, 1983). These lower-grade greenstone belts are juxtaposed against the high-grade metamorphic rocks of the Kapuskasing Structural Zone (KSZ, Fig. 2), which is bounded to the southeast by the Ivanhoe Lake Fault Zone. The Kapuskasing uplift, which separates the Wawa and Abitibi subdomains, represents a complete cross-section through the ~2.7 Ga crust and covers a range of metamorphic grades, from greenschist to granulite facies rocks (Percival and West, 1994). This region is termed the Kapuskasing "uplift" because it has been interpreted to reflect a tilted block of contiguous crust; this is best exemplified by seismic reflection indicators and apparent palaeo-pressure and -temperature values increasing toward the Ivanhoe Lake Fault Zone (ILFZ), observed in a NNE-trend of relatively high pressure in the central Kapuskasing structural zone (KSZ; Percival, 1983; Percival & West, 1994).

The Kapuskasing uplift is therefore an exemplary study location for the investigation of the deep crust, and it has been used as a natural laboratory to study heat production in the Archaean crust (Rudnick and Fountain, 1995), melting reactions and metamorphic conditions during genesis of Archaean trondhjemite-tonalites (Hartel and Pattison, 1996) and recently, the evolution of Archaean felsic crust from TTG zircons across a crustal cross-section (Kendrick et al., 2023). For the purposes of our study, this region is ideal, as the Kapuskasing preserves *in situ* melting features in its mafic migmatites and contains amphibolites inferred to represent the source material for TTGs in the area. This locality is also suitable for the study of Si isotopes because the Kapuskasing

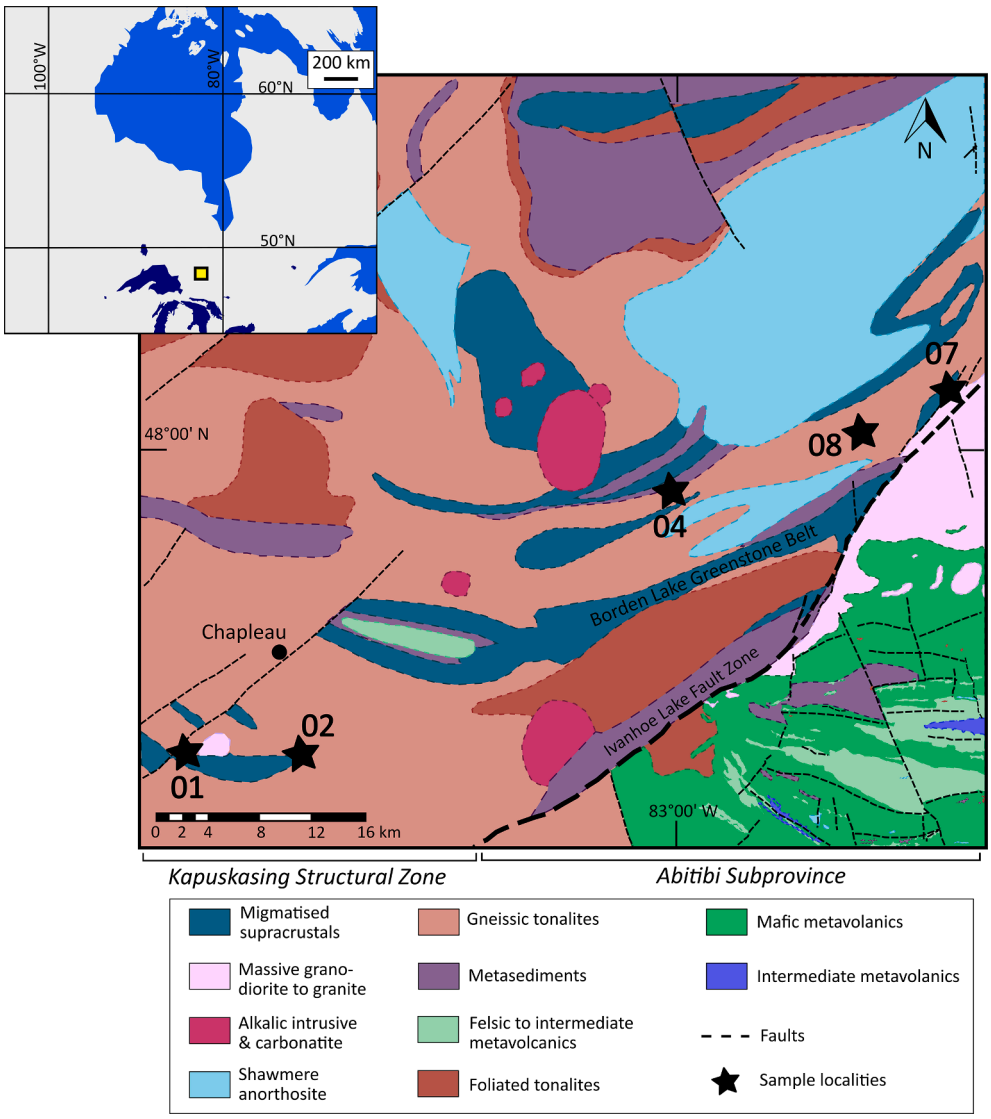

Fig. 2. Simplified sketch map of the localities where samples were collected (black stars) and the geology of the southern Kapuskasing Structural Zone (KSZ, modified after Estrada et al., 2018; Ontario Geological Survey, 2011).

uplift is a terrane devoid of chert horizons, allowing us to study the igneous rocks analogous to TTG source material without the presence of Si-rich sedimentary material. While the nearby Abitibi greenstone belt contains abundant Neoarchaean cherts and silicified volcanics which have been analysed for Si and O isotopes (Brengman et al., 2020), these supracrustal rocks are not associated with the deeper crustal KSZ, which is comprised mainly of migmatitic mafic gneiss and paragneiss, tonalites, and anorthosites (Percival, 1983; see Fig. 2).

We analysed Si isotopes in amphibolite and granulite facies rocks, including the Kapuskasing mafic migmatites that have been well-studied to establish a metamorphic history and determine *P-T* conditions for this region (Hartel & Pattison, 1996; Mäder et al., 1994; Percival, 1983). The migmatites are inferred to have been produced by dehydration melting reactions consuming amphibole, with extent of melting controlled by the abundance of quartz in the protoliths, which ultimately reached peak metamorphic conditions somewhere around 850 °C and 11 kbar (Hartel & Pattison, 1996). We have selected representative samples of leucosome, melanosome, amphibolite, and leucosome-free mafic granulite from this region, and below is a brief description of the mineral compositions of the Kapuskasing samples analysed here.

2.2. Samples

A total of eight whole-rock samples collected from the Kapuskasing uplift, as well as 12 mineral separates from these rocks, were analysed for silicon isotopes. Fig. 3 depicts field photographs of all samples analysed in this study. These comprise two amphibolites (13 Kap 01A and 01B) from southwest of Chapleau township, as well as mafic granulites (13 Kap 07A and 07B) and migmatites (13 Kap 08A$_{pure}$ and 08C), from northeast of the Borden Lake Greenstone Belt (Fig. 2). Two tonalites from the Kapuskasing Uplift (12 Kap 02A and 04) were also measured for silicon isotopes to compare with Archaean TTGs in the literature.

Amphibolite samples 01A and 01B are mainly composed of hornblende and plagioclase feldspar, as well as varying amounts of biotite (see Fig. S1 for photomicrographs); both samples were collected from the same outcrop, from areas with foliations of variable steepness (see Fig. 3). Mafic granulite 07A contains the high pressure (HP) granulite facies assemblage of plagioclase, clinopyroxene, hornblende, and garnet (Fig. S1). Sample 07B is a banded mafic granulite dominated by hornblende and plagioclase with minor clinopyroxene and no garnet. Neither of the mafic granulites show evidence of having undergone substantial partial melting or melt loss (i.e., they are not migmatitic), they are

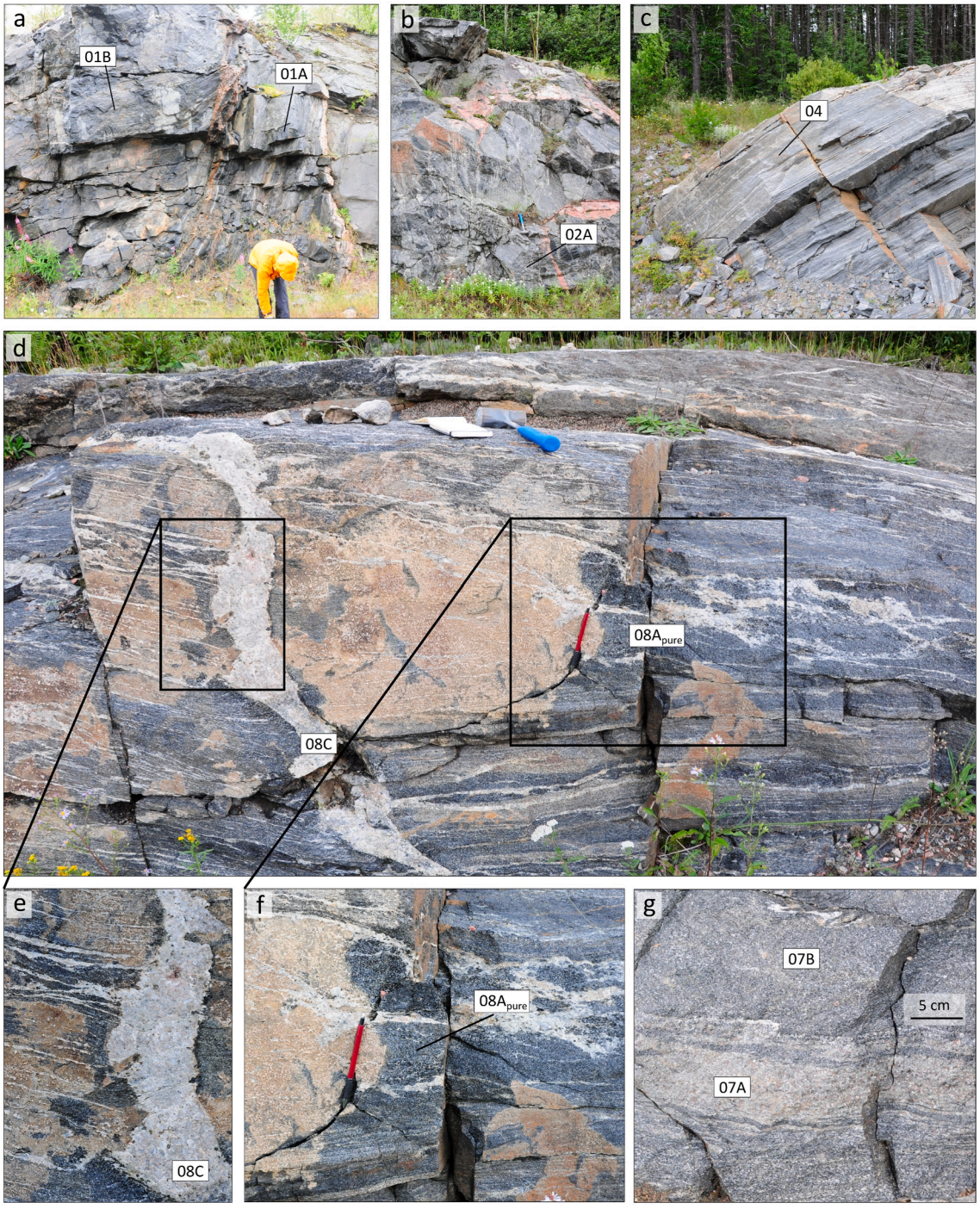

Fig. 3. Field photographs of the Kapuskasing samples analysed in this study, taken by S. Fischer during a field campaign in 2013. For localities see Fig. 2. All samples have the prefix "13 Kap", which has been omitted from the images for simplicity. a) Samples 01A and 01B come from the same outcrop in the amphibolite facies portion of the section. 01B represents the shallowly-dipping foliation reflecting the regional trend, while 01A comes from a narrow 2–3 m wide shear zone with more steeply-dipping foliation that wraps around and overprints the shallow foliation of 01B; b) An outcrop of several, broadly tonalitic lithologies. Xenoliths of amphibolitic material are hosted within felsic tonalite with steeply-dipping foliation, overprinted by a shallowly-dipping fabric at the top and bottom of the outcrop. Sample 02A was taken from the tonalite with the older, steep foliation. Note ~40 cm long blue hammer for scale; c) Sample 04 comes from an outcrop of intermediate, tonalitic gneiss with well-developed and pervasive mylonitic foliation; d) Outcrop-scale photo of field relationships for the migmatite from which components 08A and 08C were collected. Note that leucosome from the migmatite (sample 08A) feeds into the ~20 cm-wide felsic melt channel (08C).; e) Inset of 3d, showing leucosomes from within the mafic migmatite are in petrographic continuity with the melt channel (sample 08C); f) Inset of 3d, showing migmatite sample 08A (right of pen) that contains small, cm-sized leucosomes that feed into 08C; for this study, the two obvious leucosomes were cut away and only the mafic melanosome portion comprises sample 08A$_{pure}$; g) Locality 7 is an outcrop of compositionally banded mafic gneiss. Despite being in the granulite facies portion of the section, there is little sign of extensive partial melting. Photo shows relationship between the two types of mafic gneiss, 07A (lighter, garnet-cpx-rich layer) and 07B (darker, garnet-poor, amphibole-rich layer).

leucosome-free, and they have normative mineralogies representative of equilibrium mafic melt assemblages. Sample $08A_{pure}$ is the isolated melanosome of a mafic migmatite (with all leucosome cut away) and it contains largely plagioclase, clinopyroxene, and garnet, as well as minor hornblende (less abundant due to its breakdown during melting) and quartz. Sample 08C is from a ~ 20 cm wide felsic sheet (leucosome) that crosscuts the foliation of the mafic migmatite 08A; the smaller leucosomes of sample 08A feed into 08C. This leucosome is dominantly composed of plagioclase and quartz, with peritectic clinopyroxene and garnet (see Fig. S1) that were also selected for Si isotope analysis. All Kapuskasing whole-rock samples analysed here are plotted against comparable Archaean rocks such as unsilicified basalts (Abraham et al., 2011), migmatised amphibolites (Nédélec et al., 2012), and TTGs (André et al., 2019) to compare major element and Si isotope trends. These are depicted in Figs. S3 and S4 of the Appendix A.

3. Methods

3.1. Sample preparation

To prepare samples for Si isotope analysis, they were first crushed to a gravel-sized crushate and processed through a series of sieves (size fractions ranging from >2 mm to <355 μm). The 355 μm–1 mm fractions were then inspected under an optical microscope so ~10 mg each of quartz, plagioclase, clinopyroxene, hornblende, and garnet could be picked and collected separately. These separates were then powdered using an agate pestle and mortar to ready them for processing through Si isotope chemistry. Using a ball mill, whole-rock samples were milled to a fine, homogeneous powder. Major element compositions of the whole-rock samples were measured via energy-dispersive x-ray fluorescence (XRF) at the University of St Andrews using a SPECTRO XEPOS HE spectrometer to analyse glass beads made by fusing 500 mg of sample powder with 5 g lithium borate flux at 1050 °C in platinum crucibles.

3.2. Si isotope geochemistry

To ensure final solutions of 10–30 ppm Si for isotope analysis, mineral separate and powdered bulk samples were first prepared for alkali fusion following the methodologies described in Georg et al. (2006) and Savage and Moynier (2013), starting out by weighing ~10 mg of sample into 99.99 % pure Ag crucibles. Roughly 200 mg (two pellets) of 99.99 % semiconductor grade NaOH flux (Honeywell) was added to each crucible, as this flux adds only Na^+ ions to the final solution and ensures >95 % sample recovery during fusion. Crucibles containing samples and flux were then heated in a muffle furnace for ~25 mins at 720 °C and then rapidly quenched in capped vials containing high purity water (18.2ΩM·cm resistivity, purified with a MilliQ-element, MQ-e, water deioniser). After these vials equilibrated overnight, they were placed in a 60 °C ultrasonic bath to agitate the crucibles containing sample fusion cakes to aid transfer to solution, which involved sluicing each crucible with MQ-e water multiple times before taking up all sample with a pipette and transferring to a pre-cleaned 125 mL low density polyethylene (LDPE) bottle. The sample (now in 125 mL bottle) was then diluted with more MQ-e water to reach a final Si concentration of ~15–25 ppm and acidified to 1 % HNO_3 by volume.

The Heteropoly Blue methodology was then used to check for Si concentration in each sample and confirm Si yield of >95 % by measuring samples on a Thermo Scientific Evolution 60 desktop photospectrometer calibrated to standard curves for silicon. Sample solutions were then prepared for Si isotope analysis by following a cation exchange column procedure using 1.8 mL of BioRad AG50 X12 resin (200–400 mesh, after Georg et al., 2006) in BioRad PolyPrep columns. These columns were first cleaned (following recipes outlined in Savage and Moynier, 2013; see also Murphy et al., 2022) before samples were loaded onto them to result in 10 mL solutions with 3 ppm Si for analysis on the mass spectrometer.

Silicon isotope analyses were conducted at the University of St Andrews on a Thermo Scientific Neptune Plus Multi Collector Inductively Coupled Plasma Mass Spectrometer (MC- IC- P-MS) running at either medium or high resolution, following operating parameters listed in Table S1. Samples were always bracketed by the quartz sand standard NBS28 (now NIST RM8546) using a blank-standard-blank-sample bracketing procedure to correct for instrumental blank, drift, and mass bias. Isotope voltages and ratios ($^{30}Si/^{28}Si$ and $^{29}Si/^{28}Si$) were measured in 25 rounds of 8-second integrations, the averages of which were reported in the Neptune Data Evaluation software. The voltages were blank corrected offline to calculate ratios we report here as $\delta^{30}Si$ and $\delta^{29}Si$, defined as the permil deviation from the NBS28 standard:

$$\delta^{x}Si = \left[\left(\frac{^{x}Si/^{28}Si_{sample}}{^{x}Si/^{28}Si_{NBS28}} \right) - 1 \right] \times 1000;$$

where $x = 30$ or 29. The data are mass dependent; $\delta^{30}Si$ values are approximately twice $\delta^{29}Si$ (see Fig. S2), implying no molecular interferences on the silicon isotope beams. As additional checks of data accuracy and long-term reproducibility, the external standards BHVO-2 (Hawaiian basalt, USGS), Diatomite (natural pure silica, UCSB), and GSP-2 (granodiorite, USGS) were repeatedly measured along with samples. Analyses were typically made in each session such that 6 samples were always measured along with BHVO-2 and NBS28, and the other external standards were alternated between sessions. Each sequence of samples and standards was repeated 3–5 times, so each $\delta^{30}Si$ value we report represents a mean of 3–5 measurements of the same sample aliquot.

4. Results

4.1. External standards

Regular measurement of external standards BHVO-2, Diatomite, and GSP-2 was carried out over the course of this research to examine the accuracy and precision of our sample data. We report $\delta^{30}Si$ and $\delta^{29}Si$ values for a mean of 3–5 analyses ('n') of the same sample aliquot on the MC-ICP-MS. Error is reported with two standard deviations from the mean (2 s.d.) and the standard error at the 95 % confidence level (95 % s.e.); *95 % s.e.* $= (t \times s.d.)/\sqrt{n}$, where 't' is the inverse survival function of the Student's *t*-test (for the 95 % significance level, at n–1 degrees of freedom). We find $\delta^{30}Si = -0.31 \pm 0.06$ ‰ (2 s.d., n = 18) for BHVO-2, $\delta^{30}Si = 1.25 \pm 0.07$ ‰ (2 s.d., n = 9) for Diatomite, and $\delta^{30}Si = -0.22 \pm 0.09$ ‰ (2 s.d., n = 5) for GSP-2. These data for external standards show excellent agreement with literature data (Table S2). Long-term precision is estimated to be ± 0.07 ‰ (2 s.d.) from repeat analyses of these external standards.

4.2. Whole-rock samples

Silicon isotope values for the Kapuskasing amphibolite and granulite facies rocks analysed in this study are reported in Table 1 and summarised in Fig. 4. Whole-rock $\delta^{30}Si$ compositions for amphibolites (samples 01A and 01B) are –0.17 ± 0.04 ‰ (95 % s.e., n = 5) and –0.13 ± 0.03 ‰ (95 % s.e., n = 5), whereas mafic granulites (07A and 07B) exhibit lighter Si isotope values, –0.25 ± 0.03 ‰ (95 % s.e.., n = 5) and –0.33 ± 0.04 ‰ (95 % s.e., n = 5) (Fig. 4). Notably, the two amphibolites have higher SiO_2 contents than the coeval granulites, at 52.01 wt% and 54.94 wt%, compared to ~ 48 wt%. The amphibolites also have much higher Rb, Ba, Nb, La, Ce, Zr, and Sr content compared to the granulites (Table S3).

The whole-rock $\delta^{30}Si$ value for the melanosome of the mafic migmatite (sample $08A_{pure}$) approximates those of the amphibolites, at –0.17 ± 0.03 ‰ (95 % s.e., n = 5) while the leucosome of the migmatite (sample 08C) has a resolvable higher $\delta^{30}Si$ of –0.08 ± 0.03 ‰ (95 % s.e., n = 5). Tonalitic sample 02A has a silicon isotope composition of –0.01

Table 1
Silicon isotope data for whole rock (WR) and mineral separate samples analysed in this study.

Sample	Rock type	WR or mineral	WR SiO_2 (wt%)	$\delta^{30}Si$ (‰)	2 s.d.	95 % s.e.	$\delta^{29}Si$ (‰)	2 s.d.	95 % s.e.	n
13 Kap 01A	amphibolite	WR	52.01	−0.17	0.07	0.04	−0.07	0.02	0.01	5
13 Kap 01B	amphibolite	WR	54.94	−0.13	0.06	0.03	−0.07	0.04	0.02	6
		plagioclase		−0.10	0.02	0.01	−0.03	0.06	0.04	5
		hornblende		−0.39	0.07	0.04	−0.20	0.06	0.04	5
13 Kap 02A	tonalite	WR	68.91	−0.01	0.09	0.06	0.00	0.10	0.06	5
13 Kap 04	tonalite	WR	59.78	−0.05	0.09	0.06	−0.03	0.09	0.06	5
13 Kap 07A	mafic granulite	WR	47.88	−0.25	0.05	0.03	−0.13	0.04	0.02	6
		garnet		−0.55	0.09	0.06	−0.27	0.05	0.03	5
13 Kap 07B	mafic granulite	WR	47.99	−0.33	0.07	0.04	−0.19	0.03	0.02	5
		plagioclase		−0.06	0.04	0.03	−0.03	0.03	0.02	5
		hornblende		−0.42	0.02	0.01	−0.23	0.06	0.04	5
13 Kap $08A_{pure}$	melanosome	WR	50.59	−0.17	0.05	0.03	−0.09	0.03	0.02	6
		quartz		0.09	0.07	0.04	0.05	0.04	0.02	5
		clinopyroxene		−0.34	0.04	0.02	−0.18	0.05	0.03	5
		garnet		−0.41	0.10	0.06	−0.22	0.11	0.07	5
13 Kap 08C	leucosome	WR	74.35	−0.08	0.05	0.03	−0.04	0.05	0.03	6
		quartz		−0.07	0.09	0.06	−0.02	0.03	0.02	5
		plagioclase		−0.16	0.06	0.04	−0.07	0.05	0.03	5
		clinopyroxene		−0.38	0.06	0.04	−0.19	0.04	0.02	5
		garnet		−0.54	0.05	0.03	−0.30	0.07	0.04	5

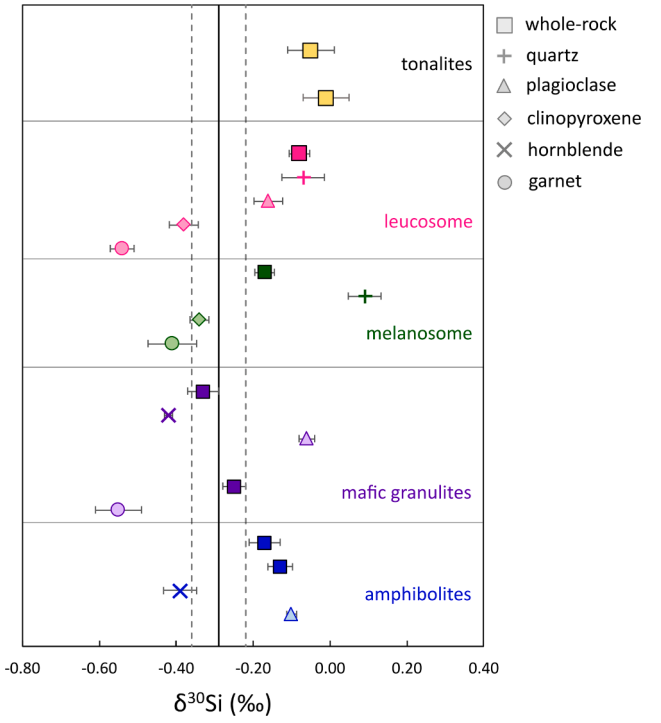

Fig. 4. Plot of silicon isotope values for our whole-rock and mineral separate samples. Error bars are 95 % standard error (s.e.). Black line and associated error (dashed grey line) is the $\delta^{30}Si$ value of the bulk silicate Earth (BSE), at –0.29 ± 0.07 ‰ (2 s.d., Savage et al., 2014).

± 0.06 ‰ (95 % s.e., n = 5) whereas the less silicic tonalite 04 has a $\delta^{30}Si$ of –0.05 ± 0.06 ‰ (95 % s.e., n = 5); these samples both plot within the silicon isotope range of Archaean TTGs reported in the literature (Fig. 1) and they are slightly isotopically heavier than our leucosome (08C).

Whole-rock Kapuskasing samples exhibit trends in major element data as well as silicon isotopes that align with comparable Archaean rocks (Figs. S3 and S4). Diagrams between silica content and other major elements indicate compositional variations resulting from magmatic differentiation (Fig. S3). Whole-rock Si isotopes in the Kapuskasing samples show a negative correlation with loss on ignition (LOI, Fig. S4), which could be interpreted to result from weathering-related clay formation, however, LOI correlates strongly with MgO but weakly with Al_2O_3, implying the trend in Si isotopes is a function of magmatic processes and/or hydration. Modal mineralogy for all samples, estimated from thin sections, is listed in Table 2, and a mass balance approximation of whole-rock $\delta^{30}Si$ values for each sample from their modal mineralogy is compared to measured $\delta^{30}Si$ values (Table 2) and depicted in Fig. 5.

4.3. Mineral separates

Si isotope values for quartz, plagioclase, hornblende, clinopyroxene, and garnet for the Kapuskasing rocks are also reported in Table 1. We find a $\delta^{30}Si$ range for quartz from –0.07 ± 0.06 ‰ (95 % s.e.) to + 0.09 ± 0.04 ‰ (95 % s.e.), with an average value of + 0.01 ± 0.07 ‰ – the isotopically heaviest of all the minerals analysed here. Plagioclase separates show an average $\delta^{30}Si$ of –0.11 ± 0.05 ‰ (95 % s.e.) and range from –0.16 ± 0.04 ‰ (95 % s.e.) to –0.06 ± 0.02 ‰ (95 % s.e.). Hornblende samples display values of –0.42 ± 0.01 ‰ (95 % s.e.) and –0.39 ± 0.04 ‰ (95 % s.e.), with clinopyroxene exhibiting an average of –0.36 ± 0.07 ‰. The isotopically lightest mineral analysed in this study is garnet, with a $\delta^{30}Si$ range from –0.55 ± 0.06 ‰ (95 % s.e.) to –0.41 ± 0.06 ‰ (95 % s.e.) and average value of –0.50 ± 0.09 ‰. Inter-mineral Si isotope fractionation factors (reported as $\Delta^{30}Si$) in these samples are estimated from the $\delta^{30}Si$ of the mineral separates and listed in Table 3.

5. Discussion

To investigate the possibility that relatively high $\delta^{30}Si$ in the earliest continental crust is a fundamental result of TTG-specific partial melting-related fractionation processes, we have analysed the component parts of a Neoarchaean migmatite for silicon isotopes. In the following discussion we address assumptions involved in interpreting these high-grade samples and consider how the Kapuskasing rocks demonstrate that partial melting has fractionated Si isotopes in a predictable fashion at least since the Archaean. We report that products of Archaean melting tend to be isotopically heavy relative to Phanerozoic analogues, implying a high- $\delta^{30}Si$ source component. We ultimately argue that the heavy Si isotope signatures of Archaean migmatites and TTGs is the result of silicification by a primeval hydrosphere.

5.1. Interpreting Si isotope results in ancient metamorphosed rocks

Prior to discussing the behaviour of silicon isotopes in the Archaean samples analysed here, it is important to address the impact of high-grade metamorphism on Si isotopes and the assumptions involved in

Table 2
Modal mineralogy estimates for the Kapuskasing amphibolites, granulites, and migmatite components for which we measured mineral separates, and a mass balance approximation of whole rock $\delta^{30}Si$ from their mineral data.

Sample	Hbl	Plag	Qtz	Grt	Cpx	Ttn	Bt	Opaques	Rock type
01B	30–40 %	45–55 %	5–10 %				<10 %	2 %	amphibolite
07A	15 %	30–40 %		20–25 %	25–30 %	5 %			mafic granulite
07B	50–60 %	25–35 %			15 %				mafic granulite
$08A_{pure}$	5 %	25–30 %	10–15 %	25–30 %	20–25 %	2 %		5 %	melanosome
08C		70–80 %	20–30 %	1 %	1 %				leucosome

Mass balance	01B	07A	07B	$08A_{pure}$	08C
qtz $\delta^{30}Si$ (‰)	0.09*	–	–	0.09	–0.07
qtz fraction	0.10	–	–	0.15	0.24
plag $\delta^{30}Si$ (‰)	–0.10*	–0.06*	–0.06	–0.06*	–0.16
plag fraction	0.50	0.35	0.30	0.30	0.74
hbl $\delta^{30}Si$ (‰)	–0.39	–0.42*	–0.42	–	–
hbl fraction	0.35	0.15	0.55	–	–
cpx $\delta^{30}Si$ (‰)	–	–0.34*	–0.34*	–0.34	–0.38
cpx fraction	–	0.27	0.15	0.25	0.01
grt $\delta^{30}Si$ (‰)	–	–0.55		–0.41	–0.54
grt fraction	–	0.23		0.30	0.01
bt $\delta^{30}Si$ (‰)	–0.33†				
bt fraction	0.05				
Predicted WR $\delta^{30}Si$(from mass balance, ‰)	–0.19 ± 0.13	–0.30 ± 0.07	–0.30 ± 0.07	–0.21 ± 0.08	–0.14 ± 0.09
Measured WR $\delta^{30}Si$ (‰)	–0.13 ± 0.03	–0.25 ± 0.03	–0.33 ± 0.04	–0.17 ± 0.03	–0.08 ± 0.03

* estimated value of mineral using data from sample with similar composition.
† Biotite Si isotope value comes from a mineral separate in TTG from André et al., 2022 (using the lowest reported value). Fractions of each mineral are based upon modal mineralogical estimates from optical microscopy (Figure S1). All WR Si isotope estimates from mass balance are within 0.06‰ of measured values. Error is 95% s.e. Titanite and opaque minerals are excluded from the mass balance as they are thought to be minor compared to the minerals that impart most of the signal to the bulk rock Si isotope value.

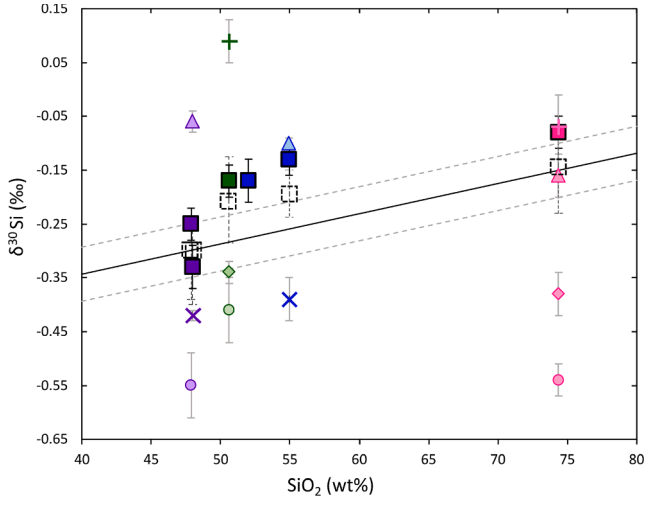

Fig. 5. Silica content against silicon isotopes in the Kapuskasing samples for which there are mineral separate data. Black dashed squares depict the predicted bulk rock values based on modal mineralogical estimates (calculations given in Table 2). All predicted bulk $\delta^{30}Si$ values are within error of their measured values, but slight offsets could be due to variable proportions of minerals in the bulk powder measured, differences in Si isotope compositions between measured minerals and those we predict in our calculations, or the relatively small sample size of our analytical sessions (n = 5). Regardless, there is strong agreement between the whole-rock values predicted from mineralogical mass balance and those we measure.

the interpretation of these data. Stable silicon isotopes are an ideal tool to assess ancient crustal samples due to their resistance to the effects of high-grade metamorphism, up to granulite facies (Savage et al., 2013). While the degree of water–rock interaction can have an impact on Si isotope compositions (e.g., extreme $\delta^{30}Si$ in late-formed serpentinite veins with high water–rock ratios; Geilert et al., 2021), the identical $\delta^{30}Si$ values in serpentinised abyssal peridotites with those of unserpentinised lherzolites (e.g. Chowdhury et al., 2023) as well as the

Table 3
Inter-mineral silicon isotope fractionation factors from the mineral separates in this study compared to *ab initio* estimates from the literature, calculated from reduced partition functions for Si isotope fractionation at 850 °C (peak metamorphic temperature after Hartel & Pattison, 1996). plag = plagioclase, hbl = hornblende, qtz = quartz, cpx = clinopyroxene, grt = garnet. [1]Qin et al., 2016; [2]Méheut and Schauble, 2014; [3]Méheut et al., 2009.

Sample	Mineral pair	Observed $\Delta^{30}Si$ (‰), this study	Propagated error (95 % s.e.)	Estimated $\Delta^{30}Si$ (‰), *ab initio* studies	Estimated error[3] (10 %)
01B	plag-hbl	0.29	0.04	0.32 (plag-diopside*)[1]	0.03
07B		0.36	0.03		
$08A_{pure}$	qtz-cpx	0.43	0.04	0.43 (qtz-diopside)[1]	0.04
08C		0.31	0.07		
$08A_{pure}$	qtz-grt	0.50	0.07	0.40 (qtz-pyrope)[2]	0.04
08C		0.47	0.07		
08C	qtz-plag	0.09	0.07	0.11 (qtz-anorthite)[1]	0.01
08C	plag-cpx	0.22	0.06	0.32 (plag-diopside)[1]	0.03
08C	plag-grt	0.38	0.05	0.35 (albite-pyrope)[2]	0.04
$08A_{pure}$	cpx-grt	0.07	0.06	0.13 (diopside-olivine*)[1]	0.01
08C		0.16	0.05		

* These assume hornblende and pyroxene as well as garnet and olivine exhibit similar temperature-dependent fractionation (e.g., Deng et al., 2019a supplementary information).

homogeneous Si isotope compositions of variably serpentinised metaperidotites (Wang et al., 2019) suggest that hydration (*sensu stricto*) has little impact on Si isotope compositions. These observations imply that the Si isotope compositions of the rocks in the present study, which have been subjected to amphibolite and granulite facies conditions with limited metasomatism (pre-migmatisation), reflect the primary

processes that shaped them rather than subsequent metamorphic overprinting.

We can also confidently preclude the effects of post-emplacement, pre-metamorphism secondary alteration on the Si isotope composition of these samples because they do not indicate formation of secondary clay minerals. Light silicon isotope signatures can be characteristic of chemical weathering-derived clay mineral neoformation (Ziegler et al., 2005; Opfergelt et al., 2012), with δ^{30}Si as low as −2.2 ‰ reported in secondary kaolinite formed from weathering of granites (Ziegler et al., 2005). However, clay Si isotope compositions can be climate-dependent, such that in subarctic conditions, weathering-derived clays can have higher δ^{30}Si, from −0.52 to −0.12 ‰ (n = 6) in cold, dry environments (Bayon et al., 2018). An average $\delta^{30}Si_{clay}$ for global weathered crust yielded a value of −0.57 ± 0.60 ‰ (2 s.d.; Bayon et al., 2018) though, which is still much isotopically lighter than our whole-rock Kapuskasing samples. While there is some overlap between our Kapuskasing rocks and clays formed in subarctic environments in plots of δ^{30}Si and alumina (Fig. 6), notably, there is no evidence for strong weathering signatures in our samples, from plots of δ^{30}Si against chemical index of alteration (CIA) and index of chemical variation (ICV; Fig. 6). Additionally, mineral separates picked for Si isotope analysis were selected under an optical microscope at 40x magnification, avoiding altered phases or those with mineral inclusions. Phases that can be difficult to pick without inclusions, like quartz, were determined by selecting very small, optically clear grains. As a check, we can also confirm from Si yield calculations during sample processing that quartz solutions contained 100 wt% SiO_2, and thus, any Si isotope signal imparted by submicroscopic mineral inclusions would be minor compared to the quartz composition (this is true for all mineral separates, i.e., their SiO_2 yields were as predicted from the mineral formulae). Careful picking of separates ensures the values we report are indicative of the freshest constituent material reflecting the primary processes that shaped these rocks.

As this study aims to understand Si isotope behaviour using data from mineral separates, another issue we must address is the assumption that for each sample the minerals analysed represent equilibrium assemblages. A first check of intra-sample mineral–mineral equilibrium is to reconstruct whole-rock δ^{30}Si values for our samples by doing a simple

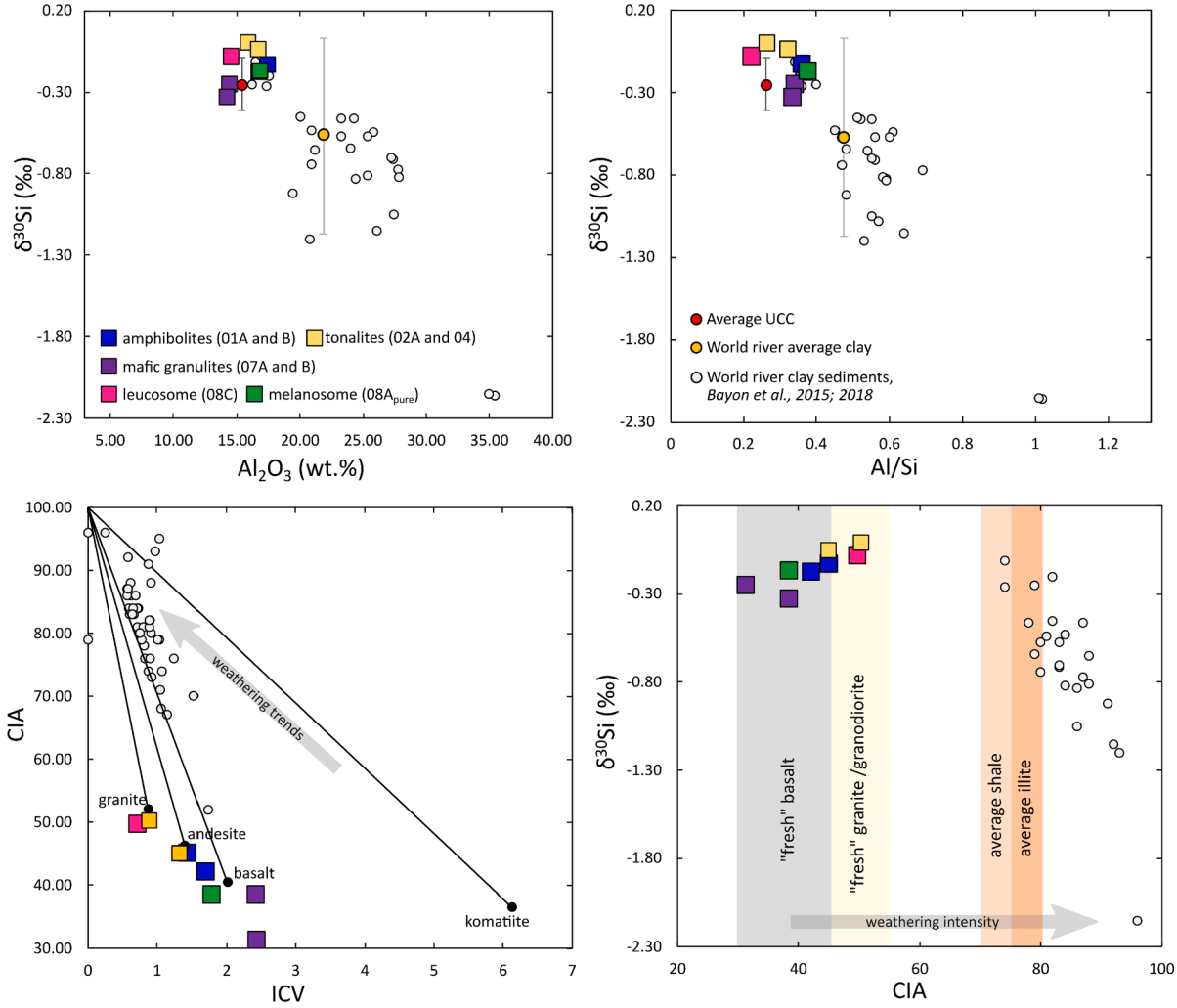

Fig. 6. Silicon isotope and major element plots to demonstrate that the whole-rock samples analysed in the present study were not influenced by secondary alteration. Top left panel shows silicon isotope values against Al_2O_3 content (wt. %) for the whole rock samples in this study, as well as world river clay sediments (from Bayon et al., 2015; 2018). The yellow circle depicts the world average river clay (δ^{30}Si value from Bayon et al., 2018; major element data from Bayon et al., 2015) and the red circle shows average upper continental crust (UCC; δ^{30}Si value from Savage et al., 2013; major element data from Rudnick and Gao, 2003), where error bars on each value are 2 s.d. Top right panel shows Si isotopes against Al/Si in the same samples, where Al/Si is a measure of the amount of secondary clay formation and progressive Si loss. Bottom right panel depicts chemical index of alteration (CIA) values for our Kapuskasing whole rocks and world river clays, as well as the typical range in unaltered igneous material, plus shales and illites (as defined by Nesbitt and Young, 1982). Higher CIA values reflect a greater degree of chemical alteration. Bottom left plot shows CIA values against index of chemical variation (ICV) values, as well as tie-lines between unaltered igneous rocks to values of CIA = 100 and ICV = 0, which depict weathering trends (after Gaschnig et al., 2016).

mass balance using estimates of sample modal mineralogy and mineral separate δ^{30}Si values (Table 2). We find a good match here between bulk analysis and "reconstructed" whole rock Si isotope composition; this confirms firstly that the mineral phases analysed appear to be in equilibrium, and, crucially, that we are not missing important Si-hosting phases. Additionally, there is careful consideration in the modelling of phase equilibria in metamorphic geology to ensure that minerals in a rock represent equilibrium assemblages, typically from textural evidence in thin section. Once equilibrium is established, these mineral assemblages can be interpreted to preserve conditions at a metamorphic peak along the *P-T* path (Powell and Holland, 2010), and the Kapuskasing assemblages have been used to estimate such peak conditions (850 °C, 11 kbar; Hartel & Pattison, 1996). It has been suggested that certain minerals, like quartz in the Kapuskasing mafic granulites, represent the products of melt crystallisation on cooling rather than solid phases at peak conditions, but that upon slow cooling of these gneisses non-uniform re-equilibration of mineral compositions would have occurred (Hartel & Pattison, 1996). For these reasons and for the simplicity of understanding Si isotope fractionation in the present study, we will operate with the assumption that our Kapuskasing samples comprise equilibrium mineral assemblages.

5.2. Si isotope fractionation during Archaean melting

While significant progress has been made to estimate inter-mineral silicon isotope fractionation over a range of pressures and temperatures via *ab initio* first-principles studies of select silicates (Méheut et al., 2009; Méheut & Schauble, 2014; Qin et al., 2016), Fe-rich phases (Rabin et al., 2021), metamorphic silicates (Yu et al., 2018; Li et al., 2019), and mantle minerals (Huang et al., 2014), this theoretical work has often not been complemented by natural samples. Although some Si isotope mineral–mineral and mineral-melt fractionation factors have been estimated from experimental (Trail et al., 2019) and natural samples (Guitreau et al., 2022; Savage et al., 2011), this study presents the first Si isotope record of *in situ* melting in mineral separates from natural Archaean samples. Fig. 7 depicts the relationship between silica content

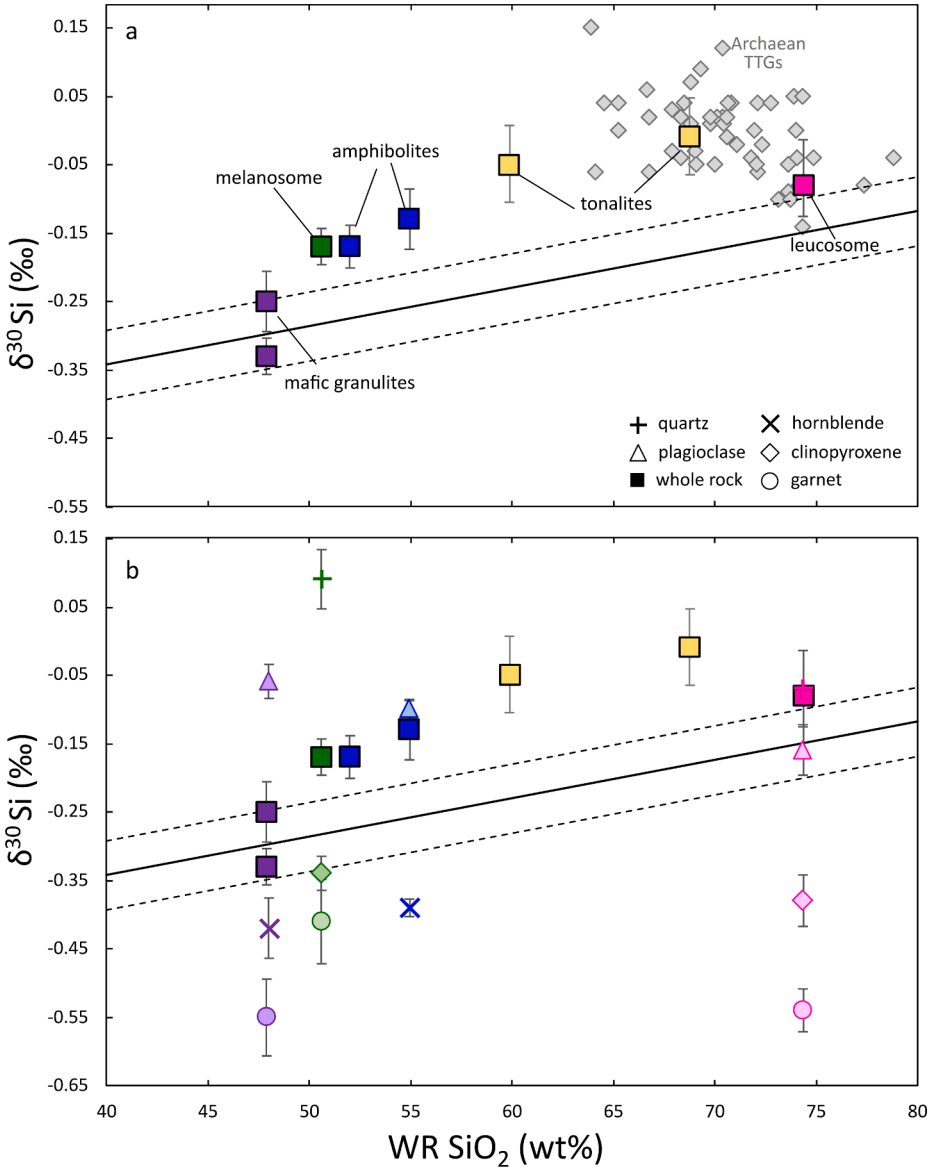

Fig. 7. Plot of δ^{30}Si against whole-rock silica content for all samples analysed in this study. Top panel depicts whole-rock samples, as well as Archaean TTGs (data as in Fig. 1). Bottom panel includes all mineral separates. Error bars are 95 % standard error. Black line and associated 2 s.e. (dashed grey lines) represent the 'igneous array' (Savage et al., 2011), the predictable relationship between silicon isotopes and silica content in Phanerozoic igneous rocks, defined by the relationship δ^{30}Si (‰) = 0.0056 × SiO_2 –0.567 (2 × s.e. of regression ± 0.05 ‰).

and $\delta^{30}Si$ in whole-rock samples in the present work along with modern analogues, and from these, the magnitude of Si isotopic fractionation between Archaean source rock and melt is comparable to that measured in Phanerozoic igneous rocks (Savage et al., 2011). Also, the inter-mineral fractionation factors derived from our mineral separates agree perfectly with those of *ab initio* estimates for Phanerozoic minerals (Table 3; e.g., Qin et al., 2016). Additionally, in Fig. 8 we show that melt-mineral fractionation factor ($\Delta^{30}Si_{melt\text{-}mineral}$) estimates for mid-ocean ridge basalt (MORB) and TTG melts at 850 °C (Deng et al., 2019a) align completely with our whole-rock-mineral fractionation factor ($\Delta^{30}Si_{WR\text{-}mineral}$) estimates (see Appendix A. Supplementary Material for a discussion of how these calculations were made). These observations imply that the effect of partial melting and magmatic differentiation on Si isotopes has remained constant since the Archaean, and we see no evidence for a mineral or selection of minerals in our samples that would explain the consistently heavy Si enrichment in TTG melts above those of Phanerozoic granitoids.

The silicon isotope values of our migmatite components also confirm theoretical predictions about Si isotope fractionation during partial melting; we report a bulk leucosome $\delta^{30}Si$ value that is 0.09 ‰ higher than that of the melanosome, demonstrating the principle that a melt will be enriched in the heavier Si isotopes compared to the residue, owing to differences in internal vibrational frequencies of Si-O bonds in coinciding phases (Grant, 1954; Méheut et al., 2009; Savage et al., 2011, 2014). Mineral separate $\delta^{30}Si$ values also illustrate this concept, as we can deconvolve the contribution of each phase to the bulk rock Si isotope composition at different SiO_2 contents. From our mineral compositions, it is evident that the Si isotope values of certain phases are fractionated to varying degrees depending on the composition of the bulk rock; for example, clinopyroxene separates are consistently isotopically light relative to whole rock $\delta^{30}Si$, yet they exhibit larger $\Delta^{30}Si_{WR\text{-}mineral}$ values in the leucosome than in the melanosome (Fig. 8) – that is, clinopyroxene is isotopically lighter in the more evolved lithology. The same is true for garnet, which exhibits its lightest Si isotope value in the leucosome, where it is interpreted to occur as a peritectic phase. It should be noted that the assumption here is that the peritectic phases must have formed at the same time as the melt (and exchanged with it), so the leucosome should be in equilibrium with these phases. Plagioclase separates also show an informative trend in this regard, as their $\delta^{30}Si$ compositions vary from isotopically heavy relative to the bulk rock in both melanosome and mafic granulite, to isotopically light compared to bulk leucosome (Fig. 8).

Our data confirm the theory that the main control on Si isotope fractionation during fractional crystallisation is the degree of polymerisation of a melt versus the minerals precipitating in that melt (Grant, 1954; Méheut et al., 2009; Méheut and Schauble, 2014). This is also reflected in the correlation between $\delta^{30}Si$ and SiO_2 as a magma evolves (Savage et al., 2010; 2011). For example, the fixed structure of plagioclase has a higher degree of polymerisation than a mafic magma (i.e., as represented by samples 07A and 07B), thus the plagioclase in this assemblage has a relatively isotopically heavy Si isotope composition compared to the whole rock (see Fig. 8). However, in a more evolved melt (i.e., leucosome), the difference in Si polymerisation between the plagioclase and melt is much smaller (than it is between plagioclase and a mafic melt), and the feldspar Si isotope value here is lighter than the whole rock (Fig. 8). A quantitative measure of the degree of polymerisation confirms this; we compare the ratio of non-bridging oxygens to tetrahedrally coordinated cations (NBO/T, after Mysen, 1983) in our whole rock samples (representing silicate melts) to the NBO/T value of representative minerals in Fig. S5 to show that, overall, the degree of polymerisation appears to exert a large control on Si isotope composition.

Note that this inference is based on fractionation of Si isotopes in magmatic/melt-bearing systems, so we directly apply this polymerisation theory to the melt-free granulite samples assuming that the sub-solidus metamorphic processes that formed them generated similar Si isotope fractionations to those that govern differences between melt and solids in igneous rocks; this is a feasible assumption given that these samples constitute equilibrium assemblages. Consequently, even though the presence of cations (namely Al^{3+}, after Méheut et al., 2009), Si-O bond length, and SiO_4 tetrahedron volume all play a role in the $\delta^{30}Si$ value of mineral phases in a melt (Qin et al., 2016), the degree of polymerisation appears to have a first-order control on equilibrium Si isotope fractionation based on the natural samples analysed in this study. Furthermore, the fact that the Si isotope compositions of mineral separates from these ~2.7 Ga samples align perfectly with both

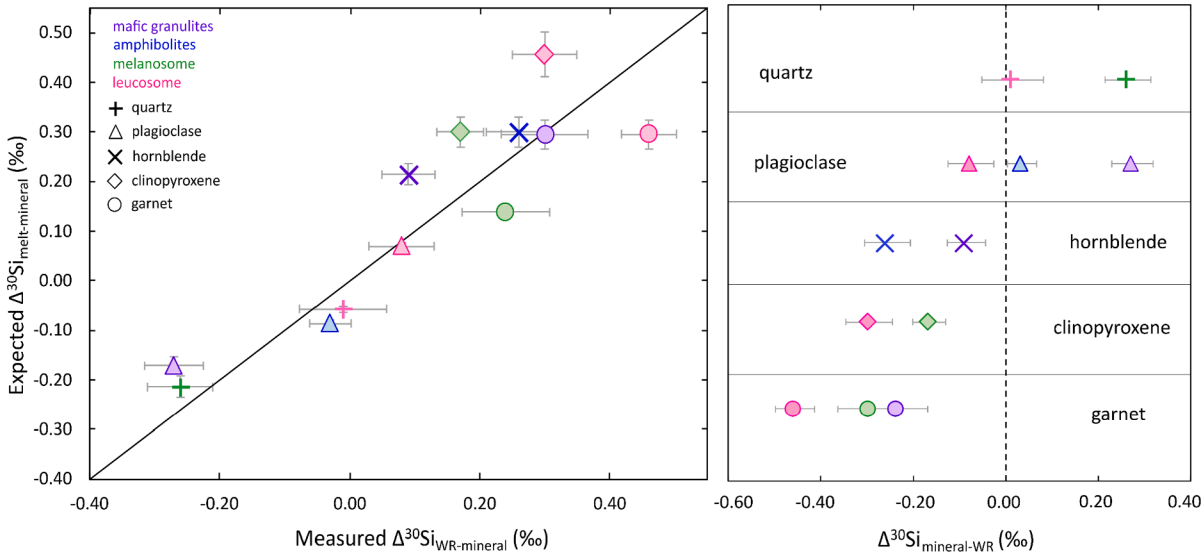

Fig. 8. Left– measured versus expected $\Delta^{30}Si_{melt/WR\text{-}mineral}$ for the mineral separates analysed in this study. Expected $\Delta^{30}Si$ values estimated from Deng et al., (2019a, Supplementary Material) for Si isotope fractionation at 850 °C in mid-ocean ridge basalt (MORB) or TTG-like melts, calculated from *ab initio* estimates (see discussion in Appendix A. Supplementary Material). This figure illustrates the good agreement of *ab initio* Si isotope fractionation factor estimates with those estimated from natural Archaean samples. Uncertainties on measured samples are propagated from 95 % s.e. on $\delta^{30}Si$ values (using root mean square error), and uncertainties on expected *ab initio* values are estimated to be 10 % (after Méheut et al., 2009; see Table 3). Right– $\Delta^{30}Si_{mineral\text{-}WR}$ for the mineral separates in this study, separated by mineral, demonstrating the relative trends where fractionation factors vary with bulk rock silica content and mineral polymerization degree.

Phanerozoic minerals and theoretical predictions suggests that melting processes have fractionated silicon isotopes in a consistent and predictable fashion at least since the Archaean.

5.3. Si isotope insights into TTG melt production

The consensus view is that TTGs form from the partial melting of hydrated basalt, however, the melting of hydrated basaltic material alone does not explain the high δ^{30}Si values seen in all Archaean TTGs (André et al., 2019; Deng et al., 2019a). As hydration (*sensu stricto*) has negligible impact on δ^{30}Si (Chowdhury et al., 2023; Wang et al., 2019), partial melting of a hydrated metabasalt (i.e., amphibolite) should, in theory, result in a more evolved rock with a silicon isotope composition identical to that of modern I- or A-type granites (cf. Savage et al., 2012; Poitrasson and Zambardi, 2015). However, hydration alone is an insufficient mechanism, as it does not account for the elevated Si isotope composition of the Kapuskasing amphibolites, and in the previous section we show that fractional crystallisation and partial melting alone do not explain the high δ^{30}Si seen in the Kapuskasing melanosome and leucosome.

Consequently, the key finding from the present study is that the addition of silica to the hydrated basaltic source material (i.e., our amphibolites and melanosome) is the crucial source of heavy Si isotope values in the melt (i.e., our leucosome). This is exemplified by the very isotopically heavy quartz in the melanosome and the heavy Kapuskasing amphibolites (01A and B) that show high silica content relative to the coeval granulites (07A and B)– which have δ^{30}Si identical to unmetamorphosed Phanerozoic basalt (e.g., Savage et al., 2010). It is apparent that, starting from the Si isotope composition of the Kapuskasing mafic granulites, it would be impossible to generate the high δ^{30}Si values seen in both the melanosome and leucosome samples (and in Archaean TTGs) from equilibrium melting processes. These instead require a source material akin to our amphibolites and melanosome with a starting composition that has heavy Si isotope values relative to both modern mafic rocks and the mafic granulites of this study; following this observation, Archaean TTG melts also necessitated a starting material with a relatively high δ^{30}Si composition.

5.3.1. The importance of silicification: solving the TTG protolith volume problem

A great deal of work has gone into understanding the starting material that partially melted to form the earliest continental crust, and one reason for the debate surrounding the geodynamic setting of Archaean TTG formation is the lack of extant basaltic material with appropriate geochemical signatures required to form these melts. The trace element characteristics of sodic TTG melts enriched in Sr and La, depleted in Y and Yb, require a mafic protolith enriched in incompatible trace elements but otherwise not dissimilar compositionally from mid-ocean ridge basalt (Jahn et al., 1981; Martin et al., 2014). However, this specific type of source material has not been identified in appropriate volumes in the Archaean rock record (Moyen & Laurent, 2018; Smithies et al., 2009; 2019). Despite this, insights from phase equilibrium modelling have helped clarify the constraints on TTG melting for different protolith compositions at various *P-T* conditions (e.g., Johnson et al., 2017; Palin et al., 2016a; 2016b; White et al., 2017). Palin et al., (2016a) showed that regardless of the type of unaltered basalt used as a protolith composition (i.e., ocean island vs. mid-ocean ridge vs. calc-alkaline types), the equilibrium phase assemblages will be essentially the same during prograde metamorphism at the *P-T* conditions that produce TTG melts; instead, the authors emphasise the control that bulk-rock water content and oxidation state exert on the variation of mineral assemblages. In other words, the debate about the type of basaltic protolith (determined by trace element signatures) appears to be secondary to the requirement that the TTG source material be hydrated.

This hydration requirement is important because it highlights the question of the source of water for TTG genesis – specifically whether TTGs formed during fluid-present or fluid-absent melting – which has been addressed by numerous phase-equilibrium studies (e.g., White et al., 2017; Palin et al., 2016b). Whether surface fluids played an integral part in the activity of water during TTG formation is also in question, with authors proposing that the release of mineral-bound water from near surface alteration in rocks like komatiites would be enough to trigger partial melting of TTG protoliths (Hartnady et al., 2022; Tamblyn et al., 2023) or that seawater played a crucial role in hydrating TTG precursors (Smithies et al., 2021; André et al., 2019; Deng et al., 2019a). The influence of seawater in the formation of Archaean TTGs has been invoked as the source of their heavy Si isotope values (André et al., 2019; Deng et al., 2019a) due to the relatively high δ^{30}Si of the ocean compared to igneous rocks. Modern seawater exhibits a Si isotope composition of around +1.5 ‰ (Sutton et al., 2018), and the δ^{30}Si composition of Precambrian seawater has been a subject of debate. If most of the dissolved Si in ancient seawater were derived from the dissolution of Archaean basaltic crust, a scenario purported by Siever (1992), its composition would approximate the bulk silicate Earth value of –0.30 ‰. More recent studies have established that Archaean marine-derived silica precipitates concentrated dissolved Si (DSi) in the global ocean with a high δ^{30}Si (e.g., Robert and Chaussidon, 2006; Sun et al., 2023), inferred to be close to or up to 2 ‰ higher than the modern value (see Fig. 1; Sun et al., 2023; Stefurak et al., 2015). This is a critical component of the present study, as the migmatite components and amphibolites exhibit high δ^{30}Si values. While dehydration melting of amphibolites is a sufficient explanation to generate TTG suites, this process alone does not explain the ubiquitously heavy silicon isotope character of these rocks, unless the specific fluid doing the hydrating is (Archaean) seawater. Hence, the interaction of basaltic source rocks with seawater presents a simple solution to this problem.

Another important element of TTG melt production is the availability of quartz. This distinction has been determined from phase-equilibrium models, which specifically show free quartz exerts a primary control on the generation of voluminous melt below 880 °C (Hartel and Pattison, 1996; Stuck and Diener, 2018) and quartz must be present in the source of modeled melts to produce siliceous, generally granitic compositions (Moyen and Stevens, 2006; Palin et al., 2016a; Palin et al., 2016b; White et al., 2017). The control exerted by free quartz on the fertility of melts has been inferred to be an important element of TTG formation in the context of silicon isotopes; André et al. (2019) postulate that a silicified mafic source (with 52–57 wt% silica content) would have been able to account for the heavy Si isotope compositions, while still abiding by melting requirements to form Archaean TTGs (i.e., protoliths with >60 wt% SiO_2 will form more silicic granodioritic to granitic melts). This hypothesis aligns completely with our Kapuskasing samples, as the high δ^{30}Si amphibolites have increased silica contents (~51–54 wt%) compared to unaltered basalt. In addition, the higher-grade counterpart to the Kapuskasing amphibolites (the equally isotopically heavy mafic migmatite) has observably generated a melt (i.e., leucosome) with a heavy Si isotope composition akin to that of all Archaean TTGs. The formation of the Kapuskasing migmatites was proposed to have occurred from the dehydration melting of amphibole wherein the abundance of quartz in the protolith was the main control on the reaction progress (Hartel & Pattison, 1996). One way to explain why some metamafic lithologies in the Kapuskasing (amphibolites 01A and 01B and the mafic migmatite 08A) melted to produce trondjhemitic melts is that their protoliths have had silica added to them, increasing their fertility and altering their silicon isotope composition; in comparison, the coeval mafic granulites without visible leucosome (07A and B) and with mantle-like δ^{30}Si values were not silicified, allowing them to reach higher metamorphic grades without undergoing partial melting.

5.3.2. Modeling the melting of a silicified protolith

We argue that an elegant solution to the issue of the source of water and free quartz – and, crucially, the high δ^{30}Si in Archaean TTGs – is seawater silicification of TTG precursors (following André et al., 2019,

2022). It is possible that the explanation for the 'missing' volume of the specific Archaean mafic material with the required incompatible element signatures is preservation bias, and these metabasaltic protoliths may have been lost to recycling or weathering, or to delamination (e.g., Bédard, 2006; Johnson et al., 2014) since the Archaean. However, seawater silicification of mafic precursors presents a solution for this TTG protolith volume problem that aligns with the established Si isotope trends as well as the observation that the exact type of basaltic material is secondary to its bulk-rock water and free quartz content in generating TTG melts. Additionally, the enrichment of elements like Rb, Ba, K, and U, along with Si, combined with the enrichment of light rare-earth elements (LREE) relative to heavy rare-earth elements (HREE) is characteristic of the low-T hydrothermal silicification of seafloor volcanics (Duchac and Hanor, 1987; Hofmann, 2005), and our Kapuskasing amphibolites share this silicification-like signature (Table S3). Furthermore, this aligns with the argument that a primitive basaltic protolith could not account for the appropriate geochemical signature of TTGs and would instead require a parent material with elevated LREE, K, and Th content relative to typical Archaean tholeiites (cf. Smithies et al., 2009).

As all the minerals in the Kapuskasing rocks appear to be in equilibrium, the heavy Si isotope values of the amphibolites and migmatite components are intrinsic properties of these rocks; there is no evidence for anomalously heavy, out-of-equilibrium phases, that could be melting to generate a TTG-precursor melt that is comparatively heavier than Phanerozoic granitoid. This implies that isotopically heavy Si was added before metamorphism into the mafic precursor package and then prograde metamorphism integrated this heavy Si into neoformed metamorphic minerals across the whole rock package. Redistribution of seawater silica throughout a mafic precursor would be more feasible for basalts silicified by a small amount of authigenic silica (after André et al., 2019) than for a protolith consisting of intercalated basalt and chert (as posited by Deng et al., 2019a). This is because large Archaean chert bands are preserved in global metamorphic terranes (e.g., Condie, 1981; Duchac & Hanor, 1987; Sugitani, 1992), and so the redistribution of all the silica from an Archaean chert to surrounding rocks seems unlikely given the fact that metamorphosed ancient cherts tend to retain their discrete structures (for example, black and white banded cherts with alternating layers of white pure chert and black carbonaceous material), and their silica can be formed by complex precipitation processes involving addition of Si during metamorphism as well diagenetic phase transformations (e.g., Stefurak et al., 2015). Further to this, even "pristine" hydrothermal chert formed on Archaean altered mafic rocks (e.g., Mount Ada Basalt) can have variable Si isotope values in veins versus its precipitated silica phases (Alleon et al., 2019). Thus, our preferred explanation for the intrinsic heavy Si isotope character of the precursors to Archaean melts is the process of silicifying and hydrating basalts on the seafloor.

This silicification process would have been ubiquitous in Archaean geodynamic settings (regardless of their specific tectonic style) due to the silica saturation of the ocean in the absence of Si-using organisms (Siever, 1992) and the low-T seafloor alteration characteristic of some Archaean hydrothermal systems (Hofmann, 2011). Although estimates for the δ^{30}Si composition of Archaean seawater exhibit a large range (see Fig. 1), we have modeled the influence of seawater silicification assuming it imparts a relatively heavy Si isotope character to the mafic TTG precursor material (Fig. 9). In doing this we hope to assess how much added marine silica would be required to generate the high δ^{30}Si values observed in Archaean melting products.

Starting with a mantle-like material characteristic of the BSE and that of our unsilicified granulite samples, Fig. 9 depicts the mixing curves we have generated with seawater silica, in increments of 10 %, to clarify the amount of silicification required to impart the values observed in high-δ^{30}Si samples. This model is intended to estimate the order of magnitude of marine silicon added to these rocks, and it is a simplified approximation, meaning that there are other nuances

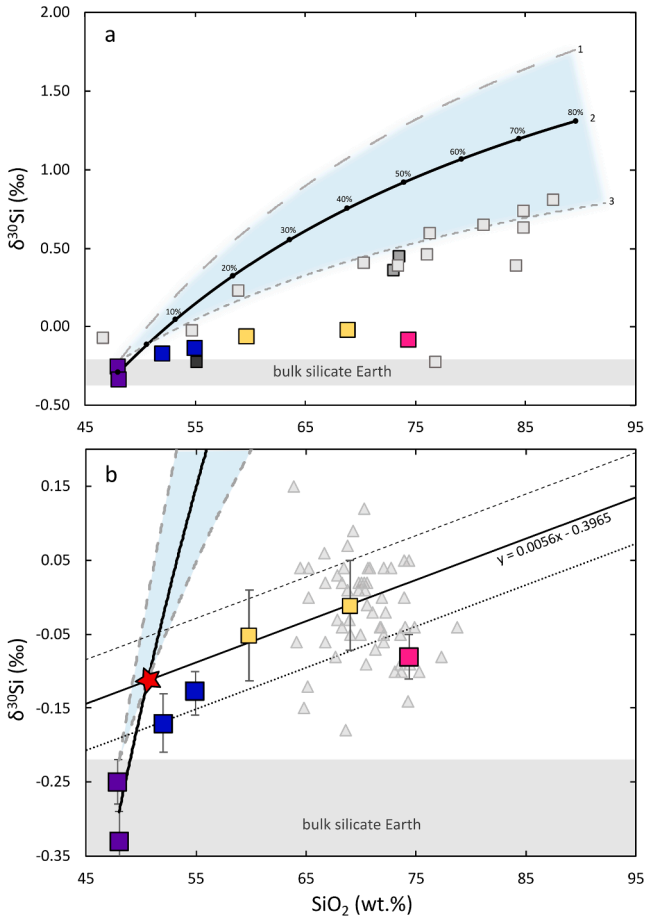

Fig. 9. a) silicon isotopes versus silica content, showing mixing curve between granulites (purple squares) and seawater. blue squares are our kapuskasing amphibolites, pink square is our leucosome, dark grey squares are silicified archaean basalts (André et al., 2019), light grey squares are silicified Archaean pillow basalts (Abraham et al., 2011), and darkest grey square is a ~2.7 Ga silicified basalt from southern Ontario (Brengman et al., 2020). The light blue envelope encompasses different estimates for Archaean seawater (endmember 1 uses a maximum $\delta^{30}Si_{seawater}$ value of +2 ‰ from Sun et al., 2023; endmember 3 uses a minimum $\delta^{30}Si_{seawater}$ of 0.87 ‰ (from the intercept of a trendline defined by the silicified basalts). The black curved line depicts increments of mixing with a seawater component (endmember 2) with a δ^{30}Si of +1.5 ‰ (modern estimate, from Sutton et al., 2018). The tick marks on this curve reflect the percentage of seawater-derived silica added to the source. Grey bar represents the bulk silicate Earth value of –0.29 ± 0.07 ‰ (Savage et al., 2014). b) Silicon isotopes versus silica content with proposed 'igneous array' (after Savage et al., 2011) using a protolith (red star) with 5 % seawater silica mixed with mafic material, using the same parameters as the black curved line in a). The dotted black line represents a source with 3 % seawater silica and dashed black line represents 7 %. This proposed source better aligns with our leucosome and Archaean TTGs (grey triangles, André et al., 2019; Deng et al., 2019a) than the Phanerozoic igneous array in Fig. 4. Error bars on amphibolites and leucosome are 95 % standard error. Solid black straight line is defined by the equation $\delta^{30}Si = 0.0056 \times SiO_2 - 0.3965$ and error on this is 2 s.d (grey dashed lines).

involved in the silicification of basalts that are not taken into account by our mixing curves; namely, during silicification some of the silicon is extracted from the altered basalts themselves by hydrothermal fluids in silica alteration zones and then redeposited (e.g., Abraham et al., 2011; André et al., 2022). However, for our simplified model where we assume all silica is redistributed into neoformed minerals, we just want to broadly estimate the amount of a marine component with a heavy Si isotope composition relative to our mafic endmembers.

It is evident from this exercise that some of the Archaean silicified basalts for which there are Si isotope data (Abraham et al., 2011; André

et al., 2019) are isotopically heavier and much more silica-rich than the protolith material we propose to have melted to form TTG (the Kapuskasing amphibolites and mafic migmatite, also shown on Fig. 9a). However, it is likely that these higher-silica rocks later underwent pervasive silicification associated with fluid circulations, compared to our silicified Kapuskasing metamafic rocks, which represent a more intermediate, less silica-rich composition. Nevertheless, these Archaean silicified basalts show an interesting trend, in that they are only slightly offset to lower δ^{30}Si values (below the black mixing curve line in Fig. 9a), that could represent a lower bound on the estimate for Archaean seawater δ^{30}Si. It is possible that the bulk Si isotope composition of the Precambrian oceans represented an average of local, hydrothermal point sources that approximated the BSE and the modern seawater composition of 1.5 ‰ (from Sutton et al., 2018), so one of the mixing curves we depict on Fig. 9 is a seawater endmember with δ^{30}Si = 0.87 ‰, derived from the intercept of a trendline defined by the silicified basalt data.

Our Kapuskasing amphibolites comprise an intermediate composition between a granulite endmember (purple squares, samples 07A and B) and a seawater silica endmember with < 10 wt% more SiO_2 than the granulites. This composition is diagnostic of the "slightly" silicified rocks recently proposed to fulfill the melting and Si isotope requirements of a TTG protolith (André et al., 2022). We therefore took a composition along the mixing curve with 3–7 % added seawater silica and used this as a starting composition to see if it was possible to generate the heavy Si isotope values of TTGs (Fig. 9b). Following the same relationship between silicon isotopes and silica content observed in Phanerozoic igneous rocks (from Savage et al., 2011), we run a differentiation trend characteristic of equilibrium magmatic processes through this inferred protolith material (red star in Fig. 9b), and it aligns well with our tonalite data as well as the Si isotope composition of Archaean TTGs, and also the Kapuskasing leucosome value. It should be noted that directly comparing the leucosome to the TTGs here is an approximation, given the inherent differences between the processes that formed them. However, in Fig. 10 we model a broad partial melting process, defined by the balance of hornblende and quartz in the protolith reacting to form a melt plus peritectics, to show that the generation of a leucosome-like melt with high δ^{30}Si still requires a silicified source rock, and that the removal of peritectics and pooling of these types of melts can generate the observed Si isotope range of Archaean TTGs (Fig. 10). There is a vertical range in TTG Si isotope values in Fig. 9b that could be a result of differing proportions of silica in the mafic starting material, as posited by André et al. (2019), or it could be due to a variable δ^{30}Si values generated by hydrothermal circulations, distinct sources of marine silica, sedimentary components, or different degrees of alteration in the basaltic source rock. Regardless, from the simple mixing model it is apparent that only a small component of seawater silica (~ <10 %) with a relatively heavy Si isotope composition is required to account for the consistently high δ^{30}Si observed in Archaean TTGs.

Our mixing curves also provide an important insight into the initial motivation for this study: that TTG Si isotope compositions appear to have a relatively consistent positive offset from Phanerozoic granitoids, despite the sources of this offset involving significantly variable compositions. Specifically, although silica precipitating from Archaean seawater might have a wide range of δ^{30}Si compositions, this potential variability is buffered by the consistent Si isotope composition of basalt (at around –0.30 ‰) when only small (<10 %) degrees of silicification are occurring, as suggested by our modelling. If such extra silica has been redistributed around the rock, the predicted isotopic variability caused by a 2 ‰ range of Archaean seawater estimates, at ~5 % silicification (e.g., red star in Fig. 9b), is only ~0.20 ‰; this smaller range easily encompasses the measured variability of natural TTGs reported to date (Fig. 7). We therefore conclude that even a minor (~10 %) degree of silicification of a basaltic source by ancient seawater is sufficient to explain the ubiquitous and relatively invariant heavy Si isotope values in products of Archaean melting.

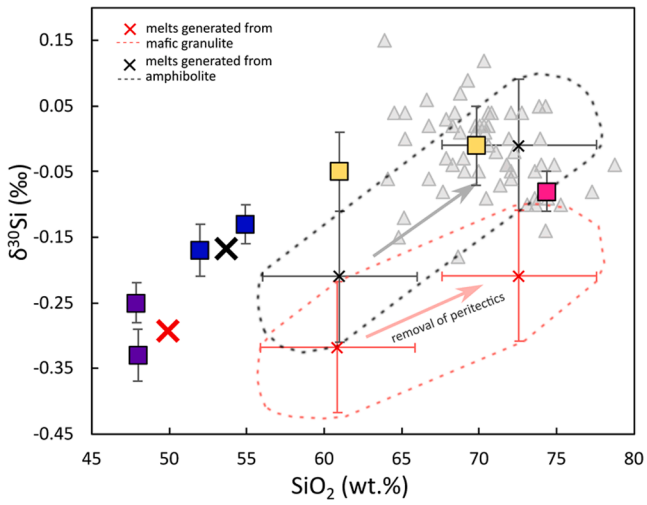

Fig. 10. Model of partial melting trends between silica content and silicon isotopes. Black dashed field shows the range of values for melt generated from silicified amphibolite (large black 'x'). Red dashed field depicts range of melt values generated from an unsilicified mafic rock (large red 'x'). This plot demonstrates that, starting with a silicified source rock, it is possible to generate the array of δ^{30}Si compositions of Archaean TTGs and the Kapuskasing leucosome, but this is not possible with a starting material similar to mafic granulite. The dashed ovular fields represent the composition of melt and peritectic phases that would be generated following one of the partial melting reactions proposed to define the Kapuskasing migmatites, from Hartel & Pattison (1996), where 1.00 Hbl + 0.72 Plag + 4.14 Qtz + 0.17 Ttn = 0.90 Grt + 1.98 Di + 1.56 Trdh. Silicon isotope values were determined by modelling a melt based on molar proportions of these phases, using mineral separate compositions from our amphibolite samples (01A and B, average bulk rock δ^{30}Si = –0.17 ‰) for the black field and predicted mineral separate values for a bulk unsilicified mafic rock (δ^{30}Si = –0.30 ‰.) for the red field. Increasing Si isotope compositions (in direction of red and black arrows) represent the removal of peritectic phases to generate a peritectic-poor melt, which for the melts generated by a silicified source rock appear to define the majority of Archaean TTGs. Our Kapuskasing leucosome is at the isotopically lighter end of the modelled range of values, which could point to the influence of its peritectic garnet and clinopyroxene. Error bars on modelled partial melts represent 2 s.d. error on Si isotope compositions and 5 wt% on silica content. Kapuskasing whole-rock and Archaean TTG symbols are as in previous figures. Detailed calculations for this figure are included in the Mendeley data file (see Data Availability section).

5.4. *Archaean geodynamic implications from Si isotopes*

The major insight into ancient geodynamics from this study is the requirement of a high δ^{30}Si source material, likely derived from seawater, in the generation of Archaean granitoid melts. Critically, our findings are based on Si isotope values in the components of migmatites that record *in situ* Archaean melting from the Kapuskasing Structural Zone, which is part of a terrane devoid of chert. This is important due to the recent inference that high δ^{30}Si values in Archaean crust must reflect the intercalation of basalts and cherts that melted to form TTGs in subduction zone settings (Deng et al., 2019a). Our data show that elevated δ^{30}Si values seem ubiquitous in Archaean felsic melts, but crucially this also occurs in the absence of chert in the rock package that is being melted. While not impossible, it is unlikely given the variability of Archaean chert δ^{30}Si values that bands of isotopically heavy chert are always present to accompany hydrated basalts during melting to form the global, ubiquitously high δ^{30}Si values observed so far in Archaean TTGs. Additionally, pure silica-rich rocks such as cherts would require unrealistically high melting temperatures compared to those involved in the melting of slightly silicified basalts; frictional melting of cherts require temperatures in excess of 1500 °C (Motohashi et al., 2019) as opposed to the melting of basalt with a free quartz enrichment that can

produce melt by 850 °C (e.g., Stuck and Diener, 2018). For these reasons, we instead propose a silicification mechanism that could occur in either a vertical tectonic setting (i.e. stacking of oceanic plateau basalts; Johnson et al., 2017; Smithies, 2000; Willbold et al., 2009) or one that invokes mobile lid tectonism (i.e. subduction; Ge et al., 2018; Hiess et al., 2009; Polat, 2012).

Our study, in agreement with the apparent consensus in the literature, invokes Precambrian seawater with a high $\delta^{30}Si$ composition that approximates or falls slightly below the composition of the modern ocean. This has interesting implications for the Archaean Si cycle; particularly, a Neoarchaean ocean with a heavy Si isotope composition would be due, in part, to subaerial continental weathering and desilication that delivered a riverine runoff with high $\delta^{30}Si$ values to the ocean, as occurs in the modern Si cycle. Precambrian seawater was postulated to have derived its silica mainly from the riverine transport flux of weathered silicates (Siever, 1992), and the appearance of detrital minerals in the rock record around 3.0–2.5 Ga suggests weathering was widespread by the late Archaean (e.g., Hessler & Lowe, 2006; Rasmussen & Buick, 1999). In this scenario, the high Si isotope composition of seawater would be accomplished via weathering of rocks like TTGs to result in clay neoformation in which the weathering fluid delivered to the ocean was enriched in ^{30}Si compared to the light neoformed clay minerals (e.g., Ziegler et al., 2005). This is corroborated by the high $\delta^{30}Si$ composition of seawater we infer from our ~2.7 Ga samples, however, Si isotope values in Mesoarchaean paleosols developed on ancient, weathered basalts do not show evidence for strong desilication or light Si isotopes in clays (Delvigne et al., 2016). It is likely that there was an increase in the amount of subaerial crust from the Meso- to Neoarchaean, associated with an increased control on the Si cycle exerted by continental weathering, however, there is mounting evidence to suggest that the Archaean marine $\delta^{30}Si$ signature was mainly controlled by high- and low-T hydrothermal fluids leaching the oceanic crust (André et al., 2006; Robert and Chaussidon, 2006; Sun et al., 2023) as well as a greater importance of buried banded iron formations (BIF) and reverse weathering (Trower and Fischer, 2019; Krissansen-Totton and Catling, 2020) that sequestered authigenic clays enriched in ^{28}Si. There is more work to be done to better constrain the inputs and outputs to the Archaean oceanic silica cycle, and particularly the role of subaerial weathering, but regardless, a heavy Si isotope composition of seawater provides a source for the ubiquitous high $\delta^{30}Si$ values in rocks shaped under the influence of the ancient hydrosphere.

Our preferred process for the generation of Archaean TTG melts is one that occurs in two steps: a basaltic material is first silicified by seawater during its extrusion and residence in the oceanic crust, from which it derives a heavy bulk Si isotope composition through the addition of silica, and this hydration *and* silicification is integrated into neoformed minerals during prograde metamorphism, which then allows (more extensive) melting to form TTGs. This agrees completely with André et al., (2019,2022), who invoke variably seawater-silicified basalts as the parent material of early felsic continental crust. Specifically, these authors cite silicified metabasalts with "relatively low silica contents" in the range of 52–57 wt% SiO_2 as the ideal source material for the anatexis that produced TTG melts (André et al., 2019; 2022), which agrees with the Kapuskasing amphibolites and migmatite. A final point to make in this regard is that these rocks have previously been interpreted to be oceanic in nature, due to possible evidence of pillow structures (Moser, 1988) and O isotope geochemistry indicative of low-T submarine alteration in the mafic gneisses (Li et al., 1991). Our Kapuskasing case study thus demonstrates the requirement of seawater silicification prior to incipient TTG melt formation and emphasises the importance of the primeval hydrosphere in the formation of the earliest continental crust.

6. Conclusions

1) We present the first estimate of Si isotope inter-mineral fractionation factors derived from mineral separates in natural Archaean samples. From these, we find Archaean Si isotope fractionation between source rock and melt and inter-mineral $\Delta^{30}Si$ values are comparable to Phanerozoic rocks and *ab initio* estimates.
2) From the similarity between Phanerozoic and Archaean samples, we infer the impact of crustal partial melting and subsequent magmatic differentiation on Si isotope behaviour has remained the same throughout Earth history.
3) Like TTGs, Archaean migmatite components (leucosome and melanosome) and coeval amphibolites exhibit high $\delta^{30}Si$ values compared to modern analogues. The high silica content of the amphibolites and heavy Si isotope character of the ocean suggest these high-$\delta^{30}Si$ rocks were silicified by Archaean, Si-saturated seawater.
4) The silicification and hydration of the amphibolite protoliths of TTGs imparted high $\delta^{30}Si$ while also ensuring these rocks were fertile enough to melt. Melting hydrated basalt alone could not generate the heavy Si isotope values observed in Archaean TTGs. Seawater silicification of basalts would have been widespread in the Archaean and provides a simple solution to the TTG protolith 'volume problem' and source of high $\delta^{30}Si$.
5) While the tectonic setting of TTG formation is still unclear, it is evident that the primeval hydrosphere played a necessary role in the formation of the earliest continental crust.

Data availability

Data are available through Mendeley Data at https://data.mendeley.com/datasets/jsstt8gm97/1.

CRediT authorship contribution statement

Madeleine E. Murphy: Conceptualization, Formal analysis, Writing – original draft. **Jane E. Macdonald:** Formal analysis. **Sebastian Fischer:** Conceptualization, Investigation, Formal analysis, Writing – review & editing. **Nicholas J. Gardiner:** Conceptualization, Writing – review & editing. **Richard W. White:** Conceptualization, Writing – review & editing. **Paul S. Savage:** Conceptualization, Funding acquisition, Writing – review & editing.

Declaration of competing interest

The authors declare that they have no known competing financial interests or personal relationships that could have appeared to influence the work reported in this paper.

Acknowledgments

We thank R. Steele for his fantastic analytical support in the STAiG lab as well as E. Stueeken for generous use of her furnace facilities at St Andrews. We would also like to thank T. Boocock and M.-A. Millet for helpful conversations with MM about the trajectory of the project. We thank reviewers L. André, M. Hartnady, and J. Marin-Carbonne for their insightful comments that greatly improved the manuscript, as well as J. Blichert-Toft for her editorial handling. This work was made possible by PhD funding to MM by the University of St Andrews School of Earth and Environmental Sciences and the Handsel scheme, in addition to NERC grant NE/R002134/1 to PS.

Appendix A. Supplementary material

PDF document containing thin section images, additional Si isotope and major element plots, tables detailing analytical settings, isotope standard data, whole-rock element contents, a partial melting model,

and a discussion of *ab initio* estimates of Si isotope fractionation factors. Supplementary material to this article can be found online at https://doi.org/10.1016/j.gca.2024.01.018.

References

Aarons, S.M., Reimink, J.R., Greber, N.D., Heard, A.W., Zhang, Z., Dauphas, N., 2020. Titanium isotopes constrain a magmatic transition at the Hadean-Archean boundary in the Acasta Gneiss Complex. Sci. Adv. 6, eabc9959.

Abraham, K., Hofmann, A., Foley, S.F., Cardinal, D., Harris, C., Barth, M.G., Andre, L., 2011. Coupled silicon–oxygen isotope fractionation traces Archaean silicification. Earth Planet. Sci. Lett. 301, 222–230.

Alleon, J., Flannery, D.T., Ferralis, N., Williford, K.H., Zhang, Y., Schuessler, J.A., Summons, R.E., 2019. Organo-mineral associations in chert of the 3.5 Ga Mount Ada Basalt raise questions about the origin of organic matter in Paleoarchean hydrothermally influenced sediments. Sci. Rep. 9, 16712.

André, L., Cardinal, D., Alleman, L.Y., Moorbath, S., 2006. Silicon isotopes in ~3.8 Ga West Greenland rocks as clues to the Eoarchaean supracrustal Si cycle. Earth Planet. Sci. Lett. 245, 162–173.

André, L., Abraham, K., Hofmann, A., Monin, L., Kleinhanns, I.C., Foley, S., 2019. (2019) Early continental crust generated by reworking of basalts variably silicified by seawater. Nat. Geosci. 129 (12), 769–773.

André, L., Monin, L., Hofmann, A., 2022. The origin of early continental crust: New clues from coupling Ge/Si ratios with silicon isotopes. Earth Planet. Sci. Lett. 582, 117415.

Bayon, G., Toucanne, S., Skonieczny, C., André, L., Bermell, S., Cheron, S., Dennielou, B., Etoubleau, J., Freslon, N., Gauchery, T., 2015. Rare earth elements and neodymium isotopes in world river sediments revisited. Geochim. Cosmochim. Acta 170, 17–38.

Bayon, G., Delvigne, C., Ponzevera, E., Borges, A., Darchambeau, F., De Deckker, P., Lambert, T., Monin, L., Toucanne, S., André, L., 2018. The silicon isotopic composition of fine-grained river sediments and its relation to climate and lithology. Geochim. Cosmochim. Acta 229, 147–161.

Bédard, J.H., 2006. A catalytic delamination-driven model for coupled genesis of Archaean crust and sub-continental lithospheric mantle. Geochim. Cosmochim. Acta 70, 1188–1214.

Bindeman, I.N., O'Neil, J., 2022. Earth's earliest hydrosphere recorded by the oldest hydrothermally-altered oceanic crust: Triple oxygen and hydrogen isotopes in the 4.3-3.8 Ga Nuvvuagittuq belt, Canada. Earth Planet. Sci. Lett. 586, 117539.

Brengman, L.A., Fedo, C.M., Whitehouse, M.J., Jabeen, I., Banerjee, N.R., 2020. Textural, geochemical, and isotopic data from silicified rocks and associated chemical sedimentary rocks in the ~ 2.7 Ga Abitibi greenstone belt, Canada: Insight into the role of silicification. Precambrian Res. 351, 105946.

Condie, K.C., 1981. Archean greenstone belts. Elsevier.

Dauphas, N., Van Zuilen, M., Wadhwa, M., Davis, A.M., Marty, B., Janney, P.E., 2004. Clues from Fe isotope variations on the origin of early Archean BIFs from Greenland. Science (80-.) 306, 2077–2080.

Delvigne, C., Opfergelt, S., Cardinal, D., Hofmann, A., André, L., 2016. Desilication in Archean weathering processes traced by silicon isotopes and Ge/Si ratios. Chem. Geol. 420, 139–147.

Deng, Z., Chaussidon, M., Guitreau, M., Puchtel, I.S., Dauphas, N., Moynier, F., 2019a. An oceanic subduction origin for Archaean granitoids revealed by silicon isotopes. Nat. Geosci. 129 (12), 774–778.

Deng, Z., Chaussidon, M., Savage, P., Robert, F., Pik, R., Moynier, F., 2019b. Titanium isotopes as a tracer for the plume or island arc affinity of felsic rocks. Proc. Natl. Acad. Sci. 116, 1132–1135.

Doucet, L.S., Laurent, O., Ionov, D.A., Mattielli, N., Debaille, V., Debouge, W., 2020. Archean lithospheric differentiation: Insights from Fe and Zn isotopes. Geology 48, 1028–1032.

Duchac, K.C., Hanor, J.S., 1987. Origin and timing of the metasomatic silicification of an early Archean komatiite sequence, Barberton Mountain Land, South Africa. Precambrian Res. 37, 125–146.

Estrada, N., Tinkham, D.K., Jorgensen, T.R.C., Marsh, J.H., 2018. Identification of partial melting relationships in the Southern Kapuskasing Structural Zone, Ontario. Summ. F Work Other Act 31.

Foley, S., Tiepolo, M., Vannucci, R., 2002. Growth of early continental crust controlled by melting of amphibolite in subduction zones. Nat. 4176891 (417), 837–840.

Ge, R., Zhu, W., Wilde, S.A., Wu, H., 2018. Remnants of eoarchean continental crust derived from a subducted proto-arc. Sci. Adv. 4.

Geilert, S., Albers, E., Frick, D.A., Hansen, C.T., von Blanckenburg, F., 2021. Systematic changes in serpentine Si isotope signatures across the Mariana forearc–a new proxy for slab dehydration processes. Earth Planet. Sci. Lett. 575, 117193.

Georg, R.B., Reynolds, B.C., Frank, M., Halliday, A.N., 2006. New sample preparation techniques for the determination of Si isotopic compositions using MC-ICPMS. Chem. Geol. 235, 95–104.

Grant, F.S., 1954. The geological significance of variations in the abundances of the isotopes of silicon in rocks. Geochim. Cosmochim. Acta 5, 225–242.

Greber, N.D., Dauphas, N., Bekker, A., Ptáček, M.P., Bindeman, I.N., Hofmann, A., 2017. Titanium isotopic evidence for felsic crust and plate tectonics 3.5 billion years ago. Science (80-.) 357, 1271–1274.

Guitreau, M., Gannoun, A., Deng, Z., Chaussidon, M., Moynier, F., Barbarin, B., Marin-Carbonne, J., 2022. Stable isotope geochemistry of silicon in granitoid zircon. Geochim. Cosmochim. Acta 316, 273–294.

Hartel, T.H.D., Pattison, D.R.M., 1996. Genesis of the Kapuskasing (Ontario) migmatitic mafic granulites by dehydration melting of amphibolite: the importance of quartz to reaction progress. J. Metamorph. Geol. 14, 591–611.

Hartnady, M.I.H., Johnson, T.E., Schorn, S., Smithies, R.H., Kirkland, C.L., Richardson, S. H., 2022. Fluid processes in the early Earth and the growth of continents. Earth Planet. Sci. Lett. 594, 117695.

Hessler, A.M., Lowe, D.R., 2006. Weathering and sediment generation in the Archean: an integrated study of the evolution of siliciclastic sedimentary rocks of the 3.2 Ga Moodies Group, Barberton Greenstone Belt, South Africa. Precambrian Res. 151, 185–210.

Hiess, J., Bennett, V.C., Nutman, A.P., Williams, I.S., 2009. In situ U-Pb, O and Hf isotopic compositions of zircon and olivine from Eoarchaean rocks, West Greenland: new insights to making old crust. Geochim. Cosmochim. Acta 73, 4489–4516.

Hoare, L., Klaver, M., Saji, N.S., Gillies, J., Parkinson, I.J., Lissenberg, C.J., Millet, M.-A., 2020. Melt chemistry and redox conditions control titanium isotope fractionation during magmatic differentiation. Geochim. Cosmochim. Acta 282, 38–54.

Hofmann, A., 2005. The geochemistry of sedimentary rocks from the Fig Tree Group, Barberton greenstone belt: Implications for tectonic, hydrothermal and surface processes during mid-Archaean times. Precambrian Res. 143, 23–49.

Hofmann, A., 2011. Archaean Hydrothermal Systems in the Barberton Greenstone Belt and Their Significance as a Habitat for Early Life BT - Earliest Life on Earth: Habitats, Environments and Methods of Detection. In (eds. S. D. Golding and M. Glikson). Springer Netherlands, Dordrecht. pp. 51–78.

Huang, F., Wu, Z., Huang, S., Wu, F., 2014. First-principles calculations of equilibrium silicon isotope fractionation among mantle minerals. Geochim. Cosmochim. Acta 140, 509–520.

Jahn, B.-M., Glikson, A.Y., Peucat, J.J., Hickman, A.H., 1981. REE geochemistry and isotopic data of Archean silicic volcanics and granitoids from the Pilbara Block, Western Australia: implications for the early crustal evolution. Geochim. Cosmochim. Acta 45, 1633–1652.

Johnson, T.E., Brown, M., Kaus, B.J.P., VanTongeren, J.A., 2014. Delamination and recycling of Archaean crust caused by gravitational instabilities. Nat. Geosci. 7, 47–52.

Johnson, T.E., Brown, M., Gardiner, N.J., Kirkland, C.L., Smithies, R.H., 2017. (2017) Earth's first stable continents did not form by subduction. Nat. 5437644 (543), 239–242.

Kendrick, J., Duguet, M., Kirkland, C.L., Liebmann, J., Lin, S., Moser, D.E., Yakymchuk, C., 2023. Anatomy of a craton: isotopic heterogeneity across an Archean crustal cross-section. Precambrian Res. 389, 107005.

Krissansen-Totton, J., Catling, D.C., 2020. A coupled carbon-silicon cycle model over Earth history: reverse weathering as a possible explanation of a warm mid-Proterozoic climate. Earth Planet. Sci. Lett. 537, 116181.

Li, H., Schwarcz, H.P., Shaw, D.M., 1991. Deep crustal oxygen isotope variations: the Wawa-Kapuskasing crustal transect, Ontario. Contrib. Mineral. Petrol. 107, 448–458.

Li, Y., Wang, W., Zhou, C., Huang, F., 2019. First-principles calculations of equilibrium silicon isotope fractionation in metamorphic silicate minerals. Solid Earth Sci. 4, 142–149.

Li, Y., Yu, H., Gu, X., Guo, S., Huang, F., 2020. Silicon isotopic fractionation during metamorphic fluid activities: constraints from eclogites and ultrahigh-pressure veins in the Dabie orogen, China. Chem. Geol. 540, 119550.

Liou, P., Wang, Z., Mitchell, R.N., Doucet, L.S., Li, M., Guo, J., Zhai, M., 2022. Fe isotopic evidence that "high pressure" TTGs formed at low pressure. Earth Planet. Sci. Lett. 592, 117645.

Mäder, U.K., Percival, J.A., Berman, R.G., 1994. Thermobarometry of garnet–clinopyroxene–hornblende granulites from the Kapuskasing structural zone. Can. J. Earth Sci. 31, 1134–1145.

Marin-Carbonne, J., Chaussidon, M., Robert, F., 2012. Micrometer-scale chemical and isotopic criteria (O and Si) on the origin and history of Precambrian cherts: implications for paleo-temperature reconstructions. Geochim. Cosmochim. Acta 92, 129–147.

Martin, H., Moyen, J.-F., Guitreau, M., Blichert-Toft, J., Le Pennec, J.-L., 2014. Why Archaean TTG cannot be generated by MORB melting in subduction zones. Lithos 198, 1–13.

Méheut, M., Lazzeri, M., Balan, E., Mauri, F., 2009. Structural control over equilibrium silicon and oxygen isotopic fractionation: A first-principles density-functional theory study. Chem. Geol. 258, 28–37.

Méheut, M., Schauble, E.A., 2014. Silicon isotope fractionation in silicate minerals: Insights from first-principles models of phyllosilicates, albite and pyrope. Geochim. Cosmochim. Acta 134, 137–154.

Moser, D., 1988. Structure of the Wawa gneiss terrane near Chapleau, Ontario. Geol. Surv. Canada Part C, 93–99.

Motohashi, G., Oohashi, K., Ujiie, K., 2019. Viscous strengthening followed by slip weakening during frictional melting of chert. Earth, Planets Sp. 71, 55.

Moyen, J.-F., Laurent, O., 2018. Archaean tectonic systems: a view from igneous rocks. Lithos 302–303, 99–125.

Moyen, J.F., Martin, H., 2012. Forty years of TTG research. Lithos 148, 312–336.

Moyen, J., Stevens, G., 2006. Experimental constraints on TTG petrogenesis: implications for Archean geodynamics. Geophys. Monogr. Geophys. Union 164, 149.

Murphy, M.E., Savage, P.S., Gardiner, N.J., Prave, A.R., Gaschnig, R.M., Rudnick, R.L., 2022. Homogenising the upper continental crust: The Si isotope evolution of the crust recorded by ancient glacial diamictites. Earth Planet. Sci. Lett. 591, 117620.

Mysen, B.O., 1983. The Structure of Silicate Melts. Annu. Rev. Earth Planet. Sci. 11, 75.

Nédélec, A., Chevrel, M.O., Moyen, J.F., Ganne, J., Fabre, S., 2012. TTGs in the making: Natural evidence from Inyoni shear zone (Barberton, South Africa). Lithos 153, 25–38.

Anon (2011) 1:250 000 scale bedrock geology of Ontario. Ontario Geol. Surv. Misc. Release- Data 126- Revis. 1.

Opfergelt, S., Georg, R.B., Delvaux, B., Cabidoche, Y.M., Burton, K.W., Halliday, A.N., 2012. Silicon isotopes and the tracing of desilication in volcanic soil weathering sequences, Guadeloupe. Chem. Geol. 326–327, 113–122.
Palin, R.M., White, R.W., Green, E.C.R., 2016a. Partial melting of metabasic rocks and the generation of tonalitic–trondhjemitic–granodioritic (TTG) crust in the Archaean: Constraints from phase equilibrium modelling. Precambrian Res. 287, 73–90.
Palin, R.M., White, R.W., Green, E.C.R., Diener, J.F.A., Powell, R., Holland, T.J.B., 2016b. High-grade metamorphism and partial melting of basic and intermediate rocks. J. Metamorph. Geol. 34, 871–892.
Percival, J.A., 1983. High-grade metamorphism in the Chapleau-Foleyet area, Ontario. Am. Mineral. 68, 667–686.
Percival J. A., Skulski T., Sanborn-Barrie M., Stott G. M., Leclair A. D., Corkery M.T., Boily M., 2012. Geology and tectonic evolution of the Superior Province, Canada. In: Tectonic styles in Canada: The LITHOPROBE perspective Geological Association of Canada Special Paper 49. pp. 321–378.
Percival, J.A., West, G.F., 1994. The Kapuskasing uplift: a geological and geophysical synthesis. Can. J. Earth Sci. 31, 1256–1286.
Poitrasson, F., Zambardi, T., 2015. An Earth-Moon silicon isotope model to track silicic magma origins. Geochim. Cosmochim. Acta 167, 301–312.
Polat, A., 2012. Growth of Archean continental crust in oceanic island arcs. Geology 40, 383–384.
Powell, R., Holland, T., 2010. Using equilibrium thermodynamics to understand metamorphism and metamorphic rocks. Elements 6, 309–314.
Qin, T., Wu, F., Wu, Z., Huang, F., 2016. First-principles calculations of equilibrium fractionation of O and Si isotopes in quartz, albite, anorthite, and zircon. Contrib. to Mineral. Petrol. 171, 91.
Rabin, S., Blanchard, M., Pinilla, C., Poitrasson, F., Gregoire, M., 2021. First-principles calculation of iron and silicon isotope fractionation between Fe-bearing minerals at magmatic temperatures: The importance of second atomic neighbors. Geochim. Cosmochim. Acta 304, 101–118.
Rapp, R.P., Watson, E.B., 1995. Dehydration Melting of Metabasalt at 8–32 kbar: Implications for Continental Growth and Crust-Mantle Recycling. J. Petrol. 36, 891–931.
Rasmussen, B., Buick, R., 1999. Redox state of the Archean atmosphere: Evidence from detrital heavy minerals in ca. 3250–2750 Ma sandstones from the Pilbara Craton, Australia. Geology 27, 115–118.
Robert, F., Chaussidon, M., 2006. A palaeotemperature curve for the Precambrian oceans based on silicon isotopes in cherts. Nature 443, 969–972.
Rudnick, R.L., Fountain, D.M., 1995. Nature and composition of the continental crust: a lower crustal perspective. Rev. Geophys. 33, 267–309.
Rumble, D., Bowring, S., Iizuka, T., Komiya, T., Lepland, A., Rosing, M.T., Ueno, Y., 2013. The oxygen isotope composition of earth's oldest rocks and evidence of a terrestrial magma ocean. Geochem. Geophys. Geosyst. 14, 1929–1939.
Savage, P.S., Georg, R.B., Williams, H.M., Turner, S., Halliday, A.N., Chappell, B.W., 2012. The silicon isotope composition of granites. Geochim. Cosmochim. Acta 92, 184–202.
Savage, P.S., Georg, R.B., Williams, H.M., Halliday, A.N., 2013. Silicon isotopes in granulite xenoliths: insights into isotopic fractionation during igneous processes and the composition of the deep continental crust. Earth Planet. Sci. Lett. 365, 221–231.
Savage, P.S., Armytage, R.M.G., Georg, R.B., Halliday, A.N., 2014. High temperature silicon isotope geochemistry. Lithos 190–191, 500–519.
Savage, P.S., Moynier, F., 2013. Silicon isotopic variation in enstatite meteorites: clues to their origin and Earth-forming material. Earth Planet. Sci. Lett. 361, 487–496.
Savage, P.S., Georg, R.B., Armytage, R.M.G., Williams, H.M., Halliday, A.N., 2010. Silicon isotope homogeneity in the mantle. Earth Planet. Sci. Lett. 295, 139–146.
Savage, P.S., Georg, R.B., Williams, H.M., Burton, K.W., Halliday, A.N., 2011. Silicon isotope fractionation during magmatic differentiation. Geochim. Cosmochim. Acta 75, 6124–6139.
Smithies, R.H., 2000. The Archaean tonalite–trondhjemite–granodiorite (TTG) series is not an analogue of Cenozoic adakite. Earth Planet. Sci. Lett. 182, 115–125.
Smithies, R.H., Champion, D.C., Van Kranendonk, M.J., 2009. Formation of Paleoarchean continental crust through infracrustal melting of enriched basalt. Earth Planet. Sci. Lett. 281, 298–306.
Smithies, R.H., Lu, Y., Johnson, T.E., Kirkland, C.L., Cassidy, K.F., Champion, D.C., Mole, D.R., Zibra, I., Gessner, K., Sapkota, J., 2019. No evidence for high-pressure melting of Earth's crust in the Archean. Nat. Commun. 10, 5559.
Smithies, R.H., Lu, Y., Kirkland, C.L., Johnson, T.E., Mole, D.R., Champion, D.C., Martin, L., Jeon, H., Wingate, M.T.D., Johnson, S.P., 2021. Oxygen isotopes trace the origins of Earth's earliest continental crust. Nature 592, 70–75.
Stefurak, E.J.T., Fischer, W.W., Lowe, D.R., 2015. Texture-specific Si isotope variations in Barberton Greenstone Belt cherts record low temperature fractionations in early Archean seawater. Geochim. Cosmochim. Acta 150, 26–52.
Stuck, T.J., Diener, J.F.A., 2018. Mineral equilibria constraints on open-system melting in metamafic compositions. J. Metamorph. Geol. 36, 255–281.
Sugitani, K., 1992. Geochemical characteristics of Archean cherts and other sedimentary rocks in the Pilbara Block, Western Australia: evidence for Archean seawater enriched in hydrothermally-derived iron and silica. Precambrian Res. 57, 21–47.
Sun, H., Chaussidon, M., Robert, F., Tian, S., Deng, Z., Moynier, F., 2023. Triple silicon isotope insights into the formation of Precambrian cherts. Earth Planet. Sci. Lett. 607, 118069.
Sutton, J.N., André, L., Cardinal, D., Conley, D.J., De Souza, G.F., Dean, J., Dodd, J., Ehlert, C., Ellwood, M.J., Frings, P.J., 2018. A review of the stable isotope bio-geochemistry of the global silicon cycle and its associated trace elements. Front. Earth Sci. 5, 112.
Tamblyn, R., Hermann, J., Hasterok, D., Sossi, P., Pettke, T., Chatterjee, S., 2023. Hydrated komatiites as a source of water for TTG formation in the Archean. Earth Planet. Sci. Lett. 603, 117982.
Trail, D., Savage, P.S., Moynier, F., 2019. Experimentally determined Si isotope fractionation between zircon and quartz. Geochim. Cosmochim. Acta 260, 257–274.
Trower, E.J., Fischer, W.W., 2019. Precambrian Si isotope mass balance, weathering, and the significance of the authigenic clay silica sink. Sediment. Geol. 384, 1–11.
van den Boorn, S.H.J.M., van Bergen, M.J., Nijman, W., Vroon, P.Z., 2007. Dual role of seawater and hydrothermal fluids in Early Archean chert formation: evidence from silicon isotopes. Geology 35, 939–942.
van den Boorn, S.H.J.M., van Bergen, M.J., Vroon, P.Z., de Vries, S.T., Nijman, W., 2010. Silicon isotope and trace element constraints on the origin of ~3.5 Ga cherts: implications for Early Archaean marine environments. Geochim. Cosmochim. Acta 74, 1077–1103.
Wang, B., Li, W.-Y., Deng, G., Huang, F., Yu, H.-M., Wang, B., Li, W.-Y., Deng, G., Huang, F., Yu, H.-M., 2019. Silicon isotope compositions of metaperidotites from the Franciscan Complex of California- implications for Si isotope fractionation during subduction dehydration. Litho 350, 105228.
White, R.W., Palin, R.M., Green, E.C.R., 2017. High-grade metamorphism and partial melting in Archean composite grey gneiss complexes. J. Metamorph. Geol. 35, 181–195.
Willbold, M., Hegner, E., Stracke, A., Rocholl, A., 2009. Continental geochemical signatures in dacites from Iceland and implications for models of early Archaean crust formation. Earth Planet. Sci. Lett. 279, 44–52.
Yu, H.-M., Li, Y.-H., Gao, Y.-J., Huang, J., Huang, F., 2018. Silicon isotopic compositions of altered oceanic crust: Implications for Si isotope heterogeneity in the mantle. Chem. Geol. 479, 1–9.
Ziegler, K., Chadwick, O.A., White, A.F., Brzezinski, M.A., 2005. δ30Si systematics in a granitic saprolite, Puerto Rico. Geology 33, 817–820.